Mechanical Systems and Signal Processing 130 (2019) 122–151

Contents lists available at ScienceDirect

Mechanical Systems and Signal Processing

journal homepage: www.elsevier.com/locate/ymssp

Recovering added mass in nanoresonator sensors from finite axial eigenfrequency data

M. Dilena [a], M. Fedele Dell'Oste [a], J. Fernández-Sáez [b], A. Morassi [a,*], R. Zaera [b]

[a] Polytechnic Department of Engineering and Architecture, University of Udine, via Cotonificio 114, 33100 Udine, Italy
[b] Department of Continuum Mechanics and Structural Analysis, Universidad Carlos III de Madrid, Av. de la Universidad 30, 28911 Leganés, Madrid, Spain

ARTICLE INFO

Article history:
Received 13 October 2018
Received in revised form 9 January 2019
Accepted 14 February 2019

Keywords:
Strain gradient theory
Nanosensors
Nanorods
Mass identification
Inverse problems
Axial vibration

ABSTRACT

In this paper we present a method for solving a finite inverse eigenvalue problem arising in the determination of added distributed mass in nanoresonator sensors by measurements of the first N natural frequencies of the free axial vibration under clamped end conditions.

The method is based on an iterative procedure that produces an approximation of the unknown mass density as a generalized Fourier partial sum of order N, whose coefficients are calculated from the first N eigenvalues. To avoid trivial non-uniqueness due to the symmetry of the initial configuration of the nanorod, it is assumed that the mass variation has support contained in half of the axis interval. Moreover, the mass variation is supposed to be small with respect to the total mass of the initial nanorod.

An extended series of numerical examples shows that the method is efficient and gives excellent results in case of continuous mass variations. The determination of discontinuous coefficients exhibits no negligible oscillations near the discontinuity points, and requires more spectral data to obtain good reconstruction. A proof of local convergence of the iteration algorithm is provided for a family of finite dimensional mass coefficients. Surprisingly enough, in spite of its local character, the identification method performs well even for not necessarily small mass changes.

To the authors' knowledge, this is the first quantitative study on the identification of distributed mass attached on nanostructures modelled within generalized continuum mechanics theories by using finite eigenvalue data.

1. Introduction

In the last years, nanosensors based on Nanoelectromechanical systems (NEMS) have gained interest in different physical, chemical and biological applications [1,2]. Enhanced capabilities have been reached by scaling down the size of the nanosensors [3,4], moving the resolution of mass detection up to the zeptogram range [5]. A kind of nanosensor of great practical interest is the mechanical nanoresonator, for which the mass sensing principle is based on monitoring the variations of the resonant frequencies caused by (unknown) additional masses attached on the surface of the initial system.

The identification problem from minimal natural frequency data of a concentrated mass (modelled, for detection purposes, as Dirac-delta point mass) located on structural elements has been addressed by Morassi and Dilena [6] for the case

* Corresponding author.
E-mail addresses: michele.dilena@uniud.it (M. Dilena), fedeledelloste.marta@spes.uniud.it (M. Fedele Dell'Oste), ppfer@ing.uc3m.es (J. Fernández-Sáez), antonino.morassi@uniud.it (A. Morassi), rzaera@ing.uc3m.es (R. Zaera).

https://doi.org/10.1016/j.ymssp.2019.02.025
0888-3270/

of rod or beams, and Rubio et al. [7] for the case of a simply supported, rectangular plate. In the above papers the classical elasticity theory was used and the added mass was considered *small* with respect to the total mass of the main structure. Moreover, Morassi and coworkers [8,9] have presented a procedure to solve the identification problem of a point mass located on the span of a rod [8] or beam [9], without any a priori assumption on the smallness of the attached mass. The latest analyses appear as auxiliary problems when a crack in a rod or beam is attempted to be identified.

Bouchaala et al. [10] presented a method to determine the position and intensity of a concentrated mass attached to the surface of an electrostatically actuated clamped-clamped microbeam used as a mass sensor. Although this last work is devoted to the study of a microsensor, the laws of classical elasticity are also used.

However, the experimental results of several authors [11–14] pointed out that the consideration of size effects in the nanoscale components could be relevant to predict their mechanical response. Therefore, since the classical continuum mechanics is a scale-free theory, other formulations based on generalized continuum mechanics approaches taking into account this size-dependent behavior, which present advantages in terms of computational cost in comparison to the molecular dynamics formulations, must be explored.

Among the generalized continuum theories, we cite here the strain gradient elasticity family including the couple stress theory [15], the first and second strain gradient theories of Mindlin [16,17], the modified couple stress theory [18] and the modified strain gradient theory [12]. The last approach, based on previous formulations of Mindlin [17] and Fleck and Hutchinson [19], needs new additional equilibrium equations to govern the behavior of higher-order stresses, and contains only three non-classical constants for isotropic linear elastic materials. This theory has been used by different authors to analyze the mechanical response of different kind of nanostructures. The interested reader can see the very recent review by Thai et al. [20].

Using the modified strain gradient theory [12], the authors analyzed for the first time the vibrational behavior of nanorods [21], Euler–Bernoulli nanobeams [22], and rectangular simply-supported Kirchhoff nanoplates [23], carrying a single point mass. For the case of small intensity of the concentrated mass, and from the properties of the eigenvalue perturbative theory, a method for the identification of the attached point mass from minimal eigenfrequency data has been also developed [21–23].

The above cited works consider concentrated masses attached to the base system. However, added distributed mass representing the adsorbed analyte seems to be more realistic in practice. In this respect much less effort to identify distributed mass on nanostructures is given until now. Nevertheless, it is worth to quote the works by Hanay et al. [24] and Bouchaala [25]. Thus, Hanay et al. [24] proposed an *inertial imaging* methodology which enables simultaneous identification of position and shape of distributed masses through real time measurements of frequency shifts of the vibrational modes of the nanosensor. Bouchaala [25] analysed the effect of a distributed added mass on the natural frequencies of an electrostatically actuated resonator modelled as a classical clamped-clamped Euler-Bernoulli beam theory with geometrical nonlinearities.

However, to the authors knowledge, a general formulation of the identification problem of distributed added mass attached on nanostructures described by generalized continuum mechanics theories is not given until now.

This paper deals with the inverse problem of determining the mass distribution of a nanorod from the knowledge of a finite number of lower natural frequencies of the axial vibration under clamped ends, assuming that the mass coefficient is *a priori known on half* of the nanorod and the added mass is a *small perturbation* of the total mass of the nanosensor.

From a mathematical point of view, this problem falls into the class of *mixed finite inverse problems* for fourth-order differential operator of the Euler–Bernoulli type, since a finite number of eigenvalues belonging to a single spectrum is known, and partial knowledge of the unknown coefficient to be determined is available. A celebrated uniqueness result for this class of inverse problems can be traced back to Hochstadt and Lieberman [26]. The result holds for second-order differential operators of Sturm–Liouville type governing the axial vibration of classical straight elastic rods, i.e., $Lv = -\frac{1}{\rho(x)} v''(x)$, for a rod with unitary axial stiffness and linear mass density $\rho(x)$. Here, $v(x)$ expresses the longitudinal displacement at x of the cross-section of the rod, $x \in [0, L]$, where L is the rod length. It is shown that if $\rho(x)$ is prescribed over $\left[\frac{L}{2}, L\right]$, then all the infinite eigenvalues under clamped end conditions $v(0) = 0 = v(L)$ suffice to determine uniquely $\rho(x)$ on $\left[0, \frac{L}{2}\right]$. It should be remarked that there is another noticeable case in which the linear mass density of the rod can be uniquely determined from the single spectrum under clamped end conditions, namely when $\rho(x)$ is symmetric about the midpoint of the interval $(0, L)$ [27].

In the case of fourth-order operators, such as the one that governs the axial vibration of a nanorod, e.g., $Lv = \frac{1}{\rho}\left(b v^{IV} - a v''\right)$, with a, b constant positive stiffness coefficients and $\rho(x)$ unknown linear mass density function (see Eq. (15) below), the results of uniqueness for $\rho(x)$ are few and require the knowledge of an even larger infinite set of eigenvalues. For example, a classic result by Barcilon [28] shows that the unique determination of the coefficients $p(x), q(x)$ of the Euler-Bernoulli operator $Lv = v^{IV} - (p(x)v')' + q(x)v$ requires knowledge of three complete spectra associated with three different boundary conditions, see the book of Gladwell [29] for a comprehensive analysis of this problem. We refer also to Schueller [30] for local uniqueness results related to an Euler-Bernoulli operator for a mixed-type inverse eigenvalue problem with two even coefficients, and to Caudill et al. [31] for the first systematic study of isospectral coefficient sets for Euler-Bernoulli operators.

In the study of the fourth-order inverse eigenvalue problem with *finite data* further difficulties occur, mainly due to the non-uniqueness of the solution and to the difficulty in obtaining error estimates on the uniform approximation of the

unknown coefficient. It can be shown that these estimates require the knowledge of infinite eigenvalues or, at least, of an accurate asymptotic formula and of sufficient spectral data to make good approximation to the infinite data, see, for example, [32]. In real cases, neither of this is available. However, despite their importance and dissemination in practical applications, general studies focused on inverse eigenvalue problems with finite data are relatively few. In this direction, the contribution by Barnes in [33] is illuminating. Barnes shows that, to deal with this class of inverse problems, it is vital to determine the weakest topology in which the available set of eigenvalues are continuous (with respect to the unknown coefficient) since, otherwise, one would attempting to extract more information from the spectral data than it contains. In [33], Barnes gives some refined approximation of the weakest topology.

With a view to these questions, and extending an idea developed in [34] for the identification of structural damage in classical full-scale rods, in this paper the finite inverse problem is investigated from a different point of view. Under the assumptions that the mass change is a *small* perturbation of the reference mass distribution of the axially vibrating nanorod, the inverse problem is linearized around the referential configuration, and frequency shifts caused by the mass change are correlated with generalized Fourier coefficients of the unknown mass variation. A numerical procedure based on an iterative first-order algorithm is proposed and a proof of local convergence of the reconstruction is provided. For the sake of completeness, it should be recalled that the idea of connecting Fourier coefficients of the unknown coefficient with frequency shifts is old and traces back to the cornerstone contribution in inverse eigenvalue theory given by Borg [35], see Hald [36] and Knobel and Lowe [37] for numerical applications.

The method has been tested on an extended class of coefficients, including smooth (e.g., continuous) and discontinuous mass variations, either with connected or disconnected support. Numerical simulations show good accuracy in approximating smooth coefficients, even in the L^∞-norm, when the first $9-12$ eigenfrequencies are used. The reconstruction of discontinuous coefficients turns out to be less accurate, especially because of non negligible oscillations of the reconstructed mass variation near the discontinuity points, and typically requires the first $15-20$ eigenfrequencies to obtain reasonable accuracy.

The plan of the paper is as follows. The formulation of the mass identification problem is presented in Section 2. Section 3 is devoted to the description of the reconstruction method. This section includes the derivation of the eigenfrequency sensitivity to added masses (Section 3.1), the linearization of the inverse problem (Section 3.2), and its use in defining the iterative procedure (Section 3.3). A proof of local convergence of the iterative method is presented in Section 4. Results of a selected set of applications of the method are illustrated in Section 5. The use of a posteriori physical filtering and the stability of identification to noise are considered in Section 5.3.4 and Section 5.3.5, respectively. Finally, for the sake of completeness, a proof of the continuity of the eigenvalues and eigenfunctions with respect to perturbations of the mass density (Theorem 3.1) is included in the "Appendix".

2. Formulation of the mass identification problem

The basis of the identification method proposed in this paper will be presented for a straight *uniform* nanorod in longitudinal vibration and under clamped end conditions. The spatial variation of the infinitesimal free longitudinal vibration of the *unperturbed* or *referential* nanorod of length L is governed by the following eigenvalue problem [38,39,21].

$$\begin{cases} b v^{IV} - a v'' = \lambda \rho_0 v, \quad x \in (0,L), & (1)\\ v(0) = 0, \;\; v''(0) = 0, & (2)\\ v(L) = 0, \;\; v''(L) = 0, & (3) \end{cases}$$

$\lambda = \omega^2$ being the eigenvalue, where ω is the (radian) frequency, and $v = v(x)$ being the corresponding eigenfunction. The coefficient $\rho_0 = const.$, $\rho_0 > 0$, represents the mass density per unit length. The coefficient $a = const.$, $a > 0$, represents the axial stiffness of the nanorod, and it can be expressed as $a = EA$, with $E, E > 0$, being the Young's modulus, and A being a geometrical parameter that may be set to correspond with the cross-sectional area of the nanorod [38]. The coefficient $b = const.$, $b > 0$, is determined as

$$b = GA\left(2l_0^2 + \frac{4}{5}l_1^2\right), \tag{4}$$

where $G = E/(2(1+\nu))$ is the shear modulus defined in terms of E and of Poisson ratio $\nu, \nu > 0$, and $l_0 > 0$, $l_1 > 0$ are length scale parameters [12,38,21].

Among the possible non-classical boundary conditions for a clamped end, those selected correspond to a nil value of the higher order axial resultant, as it has been proposed by different authors, see [38,39]. Moreover, this condition ensures the self-adjointness of the eigenvalue problem and, then, the reality of the eigenvalues [21].

It is well known that, under our assumptions, the sequence of eigenpairs $\{\lambda_n, v_n(x)\}_{n=1}^{\infty}$ of (1)–(3) is equal to

$$\lambda_n = \left(\frac{n\pi}{L}\right)^2 \left[\frac{1}{\rho_0}\left(a + b\left(\frac{n\pi}{L}\right)^2\right)\right], \tag{5}$$

$$v_n(x) = \sqrt{\frac{2}{\rho_0 L}} \sin\left(\frac{n\pi x}{L}\right), \tag{6}$$

where the following mass-normalization condition has been used

$$\int_0^L \rho_0 v_n^2(x) = 1, \quad n \geqslant 1. \tag{7}$$

Note that the sequence $\{\lambda_n\}_{n=1}^{\infty}$ of the unperturbed nanorod is *uniformly discrete*, that is, there exists a separation constant $\sigma > 0$, only depending on the parameters of the system, such that

$$|\lambda_n - \lambda_m| \geqslant \sigma, \tag{8}$$

for every $m, n \in \mathbb{N}$, with $m \neq n$. In particular, a direct calculation shows that

$$\sigma = \frac{1}{\rho_0}\left(\frac{\pi}{L}\right)^2 \left[a + 2b\left(\frac{\pi}{L}\right)^2\right]. \tag{9}$$

This property will be useful in proving the continuity of the eigenfunctions of the nanorod with respect to perturbations of the linear mass density (see the proof of Theorem 3.1 in Appendix).

Let us assume that the mass per unit length of the nanorod changes, and let us denote by

$$\rho(x) = \rho_0 + r_\epsilon(x), \quad x \in [0, L], \tag{10}$$

the mass density per unit length of the *perturbed* nanorod. We shall assume the following hypotheses on the perturbation r_ϵ:

i) (L^2-perturbation and smallness)

$$\left(\frac{1}{L}\int_0^L (r_\epsilon(x))^2 dx\right)^{\frac{1}{2}} = \epsilon\rho_0, \tag{11}$$

where the perturbation parameter ϵ is a real number such that $0 < \epsilon \leqslant \widehat{\epsilon}$, with $\widehat{\epsilon} < 1$ a small number to be chosen later on.

ii) (Regularity)

$$r_\epsilon(x) \in L^\infty([0, L]), \tag{12}$$

where $L^\infty([0, L])$ is the space of (Lebesgue measurable) functions $f : [0, L] \to \mathbb{R}$ such that $\|f\|_\infty = ess\ sup_{x\in[0,L]}|f(x)| < \infty$ almost everywhere in $[0, L]$.

iii) (Uniform lower and upper bound)

$$0 < \rho^- \leqslant \rho(x) \leqslant \rho^+, \quad x \in [0, L], \tag{13}$$

with $\rho^-, \rho^+, \rho^+ \geqslant \rho_0 + \|r_\epsilon\|_\infty$, given constants independent of ϵ.

Remark 2.1. The smallness of the mass variation $r_\epsilon(x)$ expressed in (11) allows to consider either perturbations of small amplitude given on large portions of the interval $[0, L]$ (e.g., diffuse mass change) or perturbation having large value concentrated in small parts of $[0, L]$. Moreover, it should be noticed that the mass identification problem in nanorods involves *positive* variations of the mass density ρ_0, that is

$$r_\epsilon(x) \geqslant 0, \quad x \in [0, L]. \tag{14}$$

However, it is difficult to include this constraint in our analysis, and condition (14) will be used in Section 5.3.4 to post-filtering the results of the proposed identification method.

Let us denote by $\{\lambda_n(\rho), v_n(x;\rho)\}_{n=1}^{\infty}$ the *perturbed eigenpairs* of (1)–(3) when the coefficient ρ_0 is replaced by $\rho(x)$, that is

$$\begin{cases} bv^{IV} - av'' = \lambda\rho v, & x \in (0, L), \quad (15)\\ v(0) = 0, \quad v''(0) = 0, & (16)\\ v(L) = 0, \quad v''(L) = 0. & (17) \end{cases}$$

Under our assumptions i)-iii), for any $\epsilon, 0 < \epsilon \leqslant \widehat{\epsilon}$, the eigenvalue problem (15)–(17) still maintains the properties of the unperturbed eigenvalue problem, with $0 < \lambda_1(\rho) < \ldots < \lambda_n(\rho) < \ldots, \lim_{n\to\infty}\lambda_n(\rho) = \infty$. The main goal of this paper is:

Given the unperturbed nanorod, to recover the added mass $r_\epsilon(x)$ from the knowledge of the finite eigenvalue data $\{\lambda_n(\rho)\}_{n=1}^{N}$.

Recalling that the knowledge of a single full spectrum is not enough to determine uniquely a general coefficient $r_\epsilon(x)$ (see [30] and, for Sturm-Liouville operators, [26]), here we formulate a mixed inverse problem of Hochstadt-Lieberman's type

(with finite data) in which the mass coefficient is known in half of the nanorod, namely the mass variation $r_\epsilon(x)$ has support contained in $(0, L/2)$:

$$\mathrm{supp}(r_\epsilon(x)) = \overline{\{x \in [0,L] |\ r_\epsilon(x) \neq 0\}} \subset \left(0, \frac{L}{2}\right). \tag{18}$$

3. An iterative first-order reconstruction procedure

In this section we shall present a reconstruction procedure which is inspired to the Generalized Fourier Coefficient Method introduced in [34] to deal with damage identification in (classical) beams and rods. In its essence, the method is based on the linearization of the inverse problem in a neighborhood of the referential configuration, and on using the eigenvalue sensitivity to the unknown perturbation (see next two subsections). An iterative version of the procedure will be presented in the third subsection. A formal study of the convergence is proposed in Section 4.

3.1. Eigenfrequency sensitivity to added mass

Let us introduce some notation. For any integer $m \geqslant 0$ and for any real numbers ℓ_1, ℓ_2, with $-\infty < \ell_1 < \ell_2 < +\infty$, $H^m(\ell_1, \ell_2)$ denotes the real-valued Hilbert space of the Lebesgue measurable functions $f : (\ell_1, \ell_2) \to \mathbb{R}$, such that $\int_{\ell_1}^{\ell_2} \left(f^2 + \sum_{i=1}^{m} \left(\frac{d^i f}{dx^i} \right)^2 \right) < +\infty$, where $\frac{d^i f}{dx^i}$ is the ith weak derivative of f (see, for example, [40]). We notice that, when $m = 0$, $H^0(\ell_1, \ell_2)$ coincides with the space $L^2(\ell_1, \ell_2)$ of the square integrable functions in (ℓ_1, ℓ_2), with norm $\|f\|_{L^2(\ell_1,\ell_2)} = \left(\int_{\ell_1}^{\ell_2} f^2(x) dx \right)^{\frac{1}{2}}$. In order to simplify the notation, the L^2 norm will be often denoted as $\|f\|_2$. Finally, let us set $\|f\|_\infty = \max_{x \in [0,L]} |f(x)|$ for any bounded function f, $f : [0, L] \to \mathbb{R}$. The characteristic function $\chi_I : \mathbb{R} \to \mathbb{R}$ of the closed interval I, $I \subset \mathbb{R}$, is defined as $\chi_I(x) = 1$ if $x \in I$, $\chi_I(x) = 0$ if $x \in \mathbb{R} \setminus I$.

Let us rewrite the unperturbed eigenvalue problem (1)–(3) in the following form

$$F(v(x)) = \lambda M(v(x)), \tag{19}$$

where the operators $F : H^2(0, L) \to H^2(0, L), M : H^2(0, L) \to H^2(0, L)$ are defined as

$$F(v(x)) = b v^{IV}(x) - a v''(x), \tag{20}$$

$$M(v(x)) = \rho_0 v(x). \tag{21}$$

The perturbed eigenvalue problem (15)–(17) can be described similarly, that is

$$F(v(x; \rho)) = \lambda(\rho) M_\epsilon(v(x; \rho)), \tag{22}$$

where the operator $M_\epsilon : H^2(0, L) \to H^2(0, L)$ is defined as

$$M_\epsilon(v(x; \rho)) = \rho v(x; \rho), \qquad \rho = \rho_0 + r_\epsilon. \tag{23}$$

The set $\mathcal{H}$ of admissible configurations of the clamped nanorod is given by

$$\mathcal{H} = \left\{ f : (0, L) \to \mathbb{R} \mid f \in H^2(0, L),\ f(x) = 0 \text{ at } x = 0 \text{ and at } x = L \right\}. \tag{24}$$

We introduce the following operations from $\mathcal{H} \times \mathcal{H}$ to $\mathbb{R}$:

$$\langle M(f), g \rangle = \int_0^L \rho_0 f g, \tag{25}$$

$$\langle F(f), g \rangle = \int_0^L \left(b f^{IV} - a f'' \right) g. \tag{26}$$

Integration by parts shows that both the operators M and F are self-adjoint in $\mathcal{H}_0 = \{ f : (0, L) \to \mathbb{R} \mid f \in \mathcal{H}, f''(x) = 0 \text{ at } x = 0 \text{ and at } x = L \}$., that is, $\langle M(f), g \rangle = \langle f, M(g) \rangle$ and $\langle F(f), g \rangle = \int_0^L (b f'' g'' + a f' g') = \langle f, F(g) \rangle$ for every $f,\ g \in \mathcal{H}_0$.

In the sequel, we shall use an explicit expression of the first-order perturbation (with respect to the parameter ϵ) of the eigenvalues. Note that, the nth unperturbed and perturbed eigenpair will be denoted by $\{\lambda_n, v_n(x)\}$ and $\{\lambda_n(\rho), v_n(x; \rho)\}$, respectively. In order to find the first-order change of the nth eigenvalue, we find convenient to define

$$\Delta\lambda_n = \lambda_n(\rho) - \lambda_n, \tag{27}$$

$$\Delta v_n = v_n(x; \rho) - v_n, \tag{28}$$

$$\Delta M = M_\epsilon - M, \tag{29}$$

and rewrite the normalization condition (7) as

$$\langle M(v_n), v_n\rangle = 1. \tag{30}$$

Let us multiply Eq. (19) (written for the nth unperturbed eigenfunction $v_n(x)$) and Eq. (22) (written for the nth perturbed eigenfunction $v_n(x;\rho)$) by $v_n(x;\rho)$ and $v_n(x)$, respectively. Integrating, subtracting side by side, using the self-adjointness property and condition (30), we deduce the *fundamental identity* between the states corresponding to mass coefficients ρ_0 and ρ:

$$\Delta\lambda_n = -\lambda_n\langle\Delta M(v_n), v_n\rangle - \lambda_n\langle\Delta M(\Delta v_n), v_n\rangle - \Delta\lambda_n\langle M(\Delta v_n), v_n\rangle - \Delta\lambda_n\langle\Delta M(v_n), v_n\rangle - \Delta\lambda_n\langle\Delta M(\Delta v_n), v_n\rangle. \tag{31}$$

Next, we introduce the following theorem about the continuity of eigenvalues and eigenfunctions of the problem (15)–(17) with respect to L^2-perturbations of the mass coefficient. This result will be also useful in studying the convergence of the iterative identification method presented in Section 4.

Let us denote as *a priori data* the set $\mathcal{A}$ of quantities defining the unperturbed model (e.g., the coefficients a, b, ρ_0, L), and the uniform lower and upper bound of the mass density of the perturbed model $\rho(x)$:

$$\mathcal{A} = \{a, b, \rho_0, L, \rho^-, \rho^+\}. \tag{32}$$

Note that the separation constant σ of the unperturbed nanorod depends on the a priori quantities belonging to $\mathcal{A}$, and therefore it will not be explicitly included in $\mathcal{A}$.

Theorem 3.1. *Under the above notation, let* $\rho_i(x) = \rho_0 + r_{\epsilon,i}(x)$, where $r_{\epsilon,i}(x)$ satisfies (11)–(13), $i = 1, 2$. *Let* $\{\lambda_n(\rho_i),\ v_n(x;\rho_i)\}, n \geqslant 1$, *be the nth eigenpair of (15)–(17) for* $i = 1, 2$.

For every $n \geqslant 1$, there exists a constant C_n^λ, $C_n^\lambda > 0$, only depending on the a priori data $\mathcal{A}$ *and n, such that*

$$|\lambda_n(\rho_1) - \lambda_n(\rho_2)| \leqslant C_n^\lambda \|\rho_1 - \rho_2\|_2. \tag{33}$$

Let the eigenfunctions $v_n(x;\rho_1), v_n(x;\rho_2)$ *be normalized such that*

$$\int_0^L \rho_1 v_n^2(x;\rho_1) = \int_0^L \rho_1 v_n^2(x;\rho_2) = 1 \tag{34}$$

and $v_n'(0;\rho_1)v_n'(0;\rho_2) > 0, n \geqslant 1$. *For every* $n \geqslant 1$, *there exist a number* $\widehat{\epsilon}$, $0 < \widehat{\epsilon} < 1$, *and a constant* C_n^v, $C_n^v > 0$, *both only depending on the a priori data* $\mathcal{A}$ *and n, such that*

$$\|v_n(x;\rho_1) - v_n(x;\rho_2)\|_2 \leqslant C_n^v \|\rho_1 - \rho_2\|_2, \tag{35}$$

for every ρ_1, ρ_2 *satisfying* $\|\rho_1 - \rho_2\|_2 \leqslant L^{\frac{1}{2}}\widehat{\epsilon}$.

A proof of Theorem 3.1 is presented in the Appendix.

By using inequalities (33), (35) in identity (31), for $0 < \epsilon \leqslant \widehat{\epsilon}$, the first order change with respect to ϵ of the nth eigenvalue is given by

$$\lambda_n(\rho) = \lambda_n - \lambda_n \int_0^{\frac{L}{2}} r_\epsilon(x) v_n^2(x) dx, \tag{36}$$

for every $n \geqslant 1$ and for r_ϵ satisfying (18).

To prove (36), we first start by showing that $|v_n(x)|$ is uniformly bounded in $[0, L]$ in terms of the a priori data $\mathcal{A}$ and n. By the definition of the eigenvalue problem for the unperturbed nanorod, by Hölder inequality and by using the normalization condition (7), for every $x \in [0, L]$ and every $n \geqslant 1$, we have

$$|v_n(x)| = \left|\int_0^x v_n'(s)ds\right| \leqslant L^{\frac{1}{2}}\left(\int_0^L \left(v_n'(x)\right)^2 dx\right)^{\frac{1}{2}} \leqslant \left(\frac{L}{a}\right)^{\frac{1}{2}}\left(\int_0^L \left(b\left(v_n''(x)\right)^2 + a\left(v_n'(x)\right)^2\right)dx\right)^{\frac{1}{2}} \leqslant \left(\frac{L}{a}\right)^{\frac{1}{2}}\lambda_n^{\frac{1}{2}}. \tag{37}$$

Next, we show that all the terms on the right hand side of (31), but the first, are of higher order with respect to ϵ. Let us consider the second term. By using (37), Hölder inequality and estimate (35) in Theorem 3.1, for $0 < \epsilon \leqslant \widehat{\epsilon}$, we have

$$\begin{aligned}|\lambda_n\langle\Delta M(\Delta v_n), v_n\rangle| &\leqslant \lambda_n\left|\int_0^{\frac{L}{2}} r_\epsilon(x)(v_n(x;\rho_0 + r_\epsilon) - v_n(x))v_n(x)dx\right| \leqslant \lambda_n\|v_n\|_\infty\|r_\epsilon\|_2\|v_n(x;\rho_0 + r_\epsilon) - v_n(x)\|_2 \\ &\leqslant \lambda_n\|v_n\|_\infty C_n^v\|r_\epsilon\|_2^2 \leqslant C\epsilon^2,\end{aligned} \tag{38}$$

where $C > 0$ is a constant only depending on the a priori data $\mathcal{A}$ and n.

The estimates of the third, fourth and fifth terms can be performed similarly, resulting, for $0 < \epsilon \leqslant \widehat{\epsilon}$,

$$|\Delta\lambda_n\langle M(\Delta v_n), v_n\rangle|,\ |\Delta\lambda_n\langle\Delta M(v_n), v_n\rangle| \leqslant C\epsilon^2,\ |\Delta\lambda_n\langle\Delta M(\Delta v_n), v_n\rangle| \leqslant C\epsilon^3, \tag{39}$$

where $C > 0$ is a constant only depending on the a priori data $\mathcal{A}$ and n. By using (38) and (39) in (31), and neglecting higher order terms with respect to ϵ, we obtain (36).

Let us comment the expression (36). As expected by the general theory (see, for instance, [41]), expression (36) states that addition of mass causes decrease in all the eigenvalues. More precisely, the eigenvalue shift $(\lambda_n(\rho) - \lambda_n)$ turns out to be proportional to λ_n. This fact seems to have a certain importance in the inverse problem, since the relative variation of the eigenvalues appears to be significant also for large order n. Finally, it should be noticed that the expression (36) is independent of the boundary conditions of the eigenvalue problem and, therefore, the analysis could be extended also to other sets of boundary conditions of the nanorod.

3.2. The linearized inverse problem

In this section we shall use the eigenvalue sensitivity determined in (36) to formulate a linearized version of the inverse problem and to find an approximate solution.

Using the explicit expression of the unperturbed eigenfunctions (6) in (36), we have

$$\delta\lambda_n \equiv 1 - \frac{\lambda_n(\rho)}{\lambda_n} = \int_0^{\frac{L}{2}} r_\epsilon(x)\Phi_n(x)dx, \tag{40}$$

where

$$\Phi_n(x) \equiv (v_n(x))^2 = \frac{2}{\rho_0 L}\sin^2\left(\frac{n\pi x}{L}\right), \quad n \geqslant 1. \tag{41}$$

Eq. (40) shows that the first-order relative shift of the nth eigenvalue coincides with the scalar product between the unknown mass variation $r_\epsilon(x)$ and the nth element of the family $\{\Phi_m(x)\}_{m=1}^{\infty}$.

In order to determine $r_\epsilon(x)$, a natural choice is to represent $r_\epsilon(x)$ on the family $\{\Phi_m(x)\}_{m=1}^{\infty}$ as

$$r_\epsilon(x) = \sum_{k=1}^{\infty}\beta_k\Phi_k(x)\chi_{\left[0,\frac{L}{2}\right]}, \tag{42}$$

where the convergence of the series should be understood in the mean, that is

$$\lim_{K\to\infty}\int_0^{\frac{L}{2}}\left(r_\epsilon(x) - \sum_{k=1}^{K}\beta_k\Phi_k(x)\right)^2 = 0. \tag{43}$$

The coefficients $(\beta_k)_{k=1}^{\infty}$ play the role of Generalized Fourier Coefficients of the unknown mass variation $r_\epsilon(x)$ evaluated on the family $\{\Phi_m(x)\}_{m=1}^{\infty}$. It should be noted that one cannot a priori exclude that the function $r_\epsilon(x)$ defined in (42) may change sign in the interval $(0, L/2)$; see also the remark after condition (14).

It is at this point that the a priori condition (18) can be mathematically justified. In fact, the family $\{\Phi_m(x)\}_{m=1}^{\infty}$ is a basis of the square integrable functions defined on *half* span of the nanorod, e.g., the set $L^2\left(0,\frac{L}{2}\right)$. To prove this property, we notice that the functions $\{\Phi_m(x)\}_{m=1}^{\infty}$ are *linearly independent* and form a *complete family* in $L^2\left(0,\frac{L}{2}\right)$. This last property is satisfied if, for any $r_\epsilon(x) \in L^2\left(0,\frac{L}{2}\right)$, the conditions $\int_0^{\frac{L}{2}} r_\epsilon(x)\Phi_m(x)dx = 0$ for every $n \geqslant 1$ imply $r_\epsilon(x) = 0$ in $\left(0,\frac{L}{2}\right)$. The above conditions can be rewritten as

$$0 = \int_0^{\frac{L}{2}} r_\epsilon(x)dx - \int_0^{\frac{L}{2}} r_\epsilon(x)\cos\left(\frac{2m\pi x}{L}\right)dx, \tag{44}$$

for every $m \geqslant 1$. Taking the limit in (44) as $m \to \infty$ and using the Riemann-Lebesgue Lemma (see, for instance, [42]), we have $\int_0^{\frac{L}{2}} r_\epsilon(x)dx = 0$ and, then, $\int_0^{\frac{L}{2}} r_\epsilon(x)\cos\left(\frac{2m\pi x}{L}\right)dx = 0$ for every $m \geqslant 1$. Since the family $\left\{\cos\left(\frac{2m\pi x}{L}\right)\right\}_{m=1}^{\infty}$ is a basis for the set of functions belonging to $L^2\left(0,\frac{L}{2}\right)$ and having zero-mean, we have $r_\epsilon(x) = 0$ in $\left(0,\frac{L}{2}\right)$, and the thesis is proved.

Replacing (42) in (40), we obtain the infinite linear system

$$\delta\lambda_n = \sum_{k=1}^{\infty}A_{nk}\beta_k, \quad n = 1, 2, \ldots, \tag{45}$$

where

$$A_{nk} = \int_0^{\frac{L}{2}}\Phi_n(x)\Phi_k(x)dx = \frac{4}{(\rho_0 L)^2}\int_0^{\frac{L}{2}}\sin^2\left(\frac{n\pi x}{L}\right)\sin^2\left(\frac{k\pi x}{L}\right)dx, \tag{46}$$

$n, k = 1, 2\ldots$. The coefficients A_{nk} can be evaluated in closed form, and we have

$$A_{nk} = \frac{2}{4\rho_0^2 L} \quad \text{for } k \neq n, \quad A_{nn} = \frac{3}{4\rho_0^2 L}. \tag{47}$$

In real applications only a finite number of eigenvalues is available, typically the first $10-20$. This leads us to consider the Nth finite dimensional approximation of the added mass, $(\beta_k^N)_{k=1}^N$ of (45), that is the $N\times N$ linear system

$$\delta\lambda_n=\sum_{k=1}^{N}A_{nk}\beta_k^N,\quad n=1,\dots,N. \tag{48}$$

A direct calculation shows that

$$\det(A_{nk})=(2N+1)\left(\frac{1}{4\rho_0^2L}\right)^N, \tag{49}$$

$$(A_{nk})^{-1}=(4\rho_0^2L)\frac{2N-1}{2N+1}\ \text{ if } n=k,\quad (A_{nk})^{-1}=-(4\rho_0^2L)\frac{2}{2N+1}\ \text{ if } n\neq k, \tag{50}$$

$n,k=1,\dots,M$. Therefore, the system (48) has the closed-form solution

$$\beta_k^N=4\rho_0^2L\left(\frac{2N-1}{2N+1}\delta\lambda_k-\frac{2}{2N+1}\sum_{j=1,\ j\neq k}^{N}\delta\lambda_j\right),\quad k=1,\dots,N, \tag{51}$$

and, finally,

$$r_\epsilon(x)=8\rho_0\sum_{k=1}^{N}\left(\frac{2N-1}{2N+1}\delta\lambda_k-\frac{2}{2N+1}\sum_{j=1,\ j\neq k}^{N}\delta\lambda_j\right)\sin^2\left(\frac{k\pi x}{L}\right)\cdot\chi_{\left[0,\frac{L}{2}\right]}. \tag{52}$$

3.3. The reconstruction procedure

The estimation of r_ϵ given in (52) can be improved by iterating the identification procedure illustrated in the previous section. In order to simplify the notation, here the index ϵ has been omitted and λ_n^{exp} denotes the measured value of the nth eigenvalue $\lambda_n(\rho)$ of the perturbed nanorod. Moreover, we shall write β instead of β^N. The main steps of the reconstruction procedure and the corresponding numerical algorithm are illustrated in the sequel.

Let $\rho^{(0)}(x)=\rho_0$ be the mass per unit length of the referential nanorod. The unknown mass per unit length is determined on the interval $\left[0,\frac{L}{2}\right]$ by the iteration

$$\rho^{(j+1)}(x)=\rho^{(j)}(x)+r^{(j)}(x),\quad j\geqslant 0, \tag{53}$$

where the increment

$$r^{(j)}(x)=\sum_{k=1}^{N}\beta_k^{(j)}\Phi_k^{(j)}(x)\chi_{\left[0,\frac{L}{2}\right]}=\beta^{(j)}\cdot\Phi^{(j)}(x)\chi_{\left[0,\frac{L}{2}\right]} \tag{54}$$

is determined by solving the $N\times N$ linear system

$$\delta\lambda_n^{(j)}\equiv 1-\frac{\lambda_n^{exp}}{\lambda_n(\rho^{(j)})}=\sum_{k=1}^{N}A_{nk}^{(j)}\beta_k^{(j)}, \tag{55}$$

$n=1,\dots,N$, or, equivalently, in compact form

$$\mathbf{A}^{(j)}\beta^{(j)}=\delta\lambda^{(j)}, \tag{56}$$

with $\beta^{(j)}=\left(\beta_1^{(j)},\dots,\beta_N^{(j)}\right)$. Here, $\{\lambda_n(\rho^{(j)}),v_n(x;\rho^{(j)})\}$ is the nth (mass normalized) eigenpair of the problem

$$\begin{cases} bv^{IV}-av''=\lambda\rho^{(j)}v, & x\in(0,L), \quad (57)\\ v(0)=0, & v''(0)=0, \quad (58)\\ v(L)=0, & v''(L)=0. \quad (59)\end{cases}$$

Moreover, $\Phi_k^{(j)}(x)=v_k^2(x;\rho^{(j)})$ and the matrix $\left(A_{nk}^{(j)}\right)$ is given by

$$A_{nk}^{(j)}=\int_0^{\frac{L}{2}}\Phi_n^{(j)}(x)\Phi_k^{(j)}(x)dx,\quad n,k=1,\dots,N. \tag{60}$$

Assuming the existence of $\left(\mathbf{A}^{(j)}\right)^{-1}$ (see Section 4, Step i)), we have

$$r^{(j)}(x) = \left(\mathbf{A}^{(j)}\right)^{-1} \delta\lambda^{(j)} \cdot \Phi^{(j)}(x)\chi_{[0,\frac{L}{2}]} \tag{61}$$

and, from (53), we have

$$\rho^{(j)}(x) = \rho_0 + \sum_{i=0}^{j-1} r^{(i)}(x), \quad j \geqslant 1. \tag{62}$$

In our application, the iterations go on until the updated mass coefficient satisfies the criterion

$$e \equiv \frac{1}{N}\left(\sum_{n=1}^{N}\left(\lambda_n^{exp} - \lambda_n\left(\frac{\rho^{(j+1)}}{\lambda_n^{exp}}\right)^2\right)^{\frac{1}{2}} < \gamma, \tag{63}$$

for a small given number γ.

4. Convergence of the identification method

In this section we study the convergence of the iterative method shown in Section 3.3. We prove that, under suitable assumptions, there exists $\overline{\rho}(x) \in C^0(0,\frac{L}{2})$ such that

$$\overline{\rho}(x) = \lim_{j\to\infty} \rho^{(j)}(x) = \rho_0 + \sum_{i=0}^{\infty} r^{(i)}(x), \tag{64}$$

where the series is uniformly convergent in $(0,\frac{L}{2})$.

The proof is based on two main steps:

Step i) Existence of the inverse $\left(\mathbf{A}^{(j)}\right)^{-1}$ and bound of $\|\left(\mathbf{A}^{(j)}\right)^{-1}\|$ for every $j \geqslant 1$;

Step ii) Bound of $|\delta\lambda^{(j)}|$ to control $\|r^{(i)}\|_2$ for every $j \geqslant 1$.

In the sequel, we shall denote by C positive constants which may change from line to line. Moreover, for every $N \times N$ matrix $\mathbf{B} \in \mathbb{R}^{N\times N}$, we denote by $\|\mathbf{B}\| = \left(\sum_{i,j=1}^{N}(B_{ij})^2\right)^{\frac{1}{2}}$ the Frobenius norm.

Step i). Let us consider the set of coefficients $\rho(x)$ given in (10), e.g., $\rho(x) = \rho_0 + r_\epsilon(x)$ in $[0,L]$, where r_ϵ satisfies conditions (10)–(13) and where $\epsilon > 0$ is a number small enough. We denote by $\mathbf{A}(\rho)$ the matrix defined in (60) corresponding to the coefficient $\rho(x)$.

We prove that there exists $\widehat{\epsilon}_\rho$, $0 < \widehat{\epsilon}_\rho < 1$, only depending on the a priori data $\mathcal{A}$ and N, such that, for every $\epsilon < \widehat{\epsilon}_\rho$, there exists $(\mathbf{A}(\rho))^{-1}$ and we have

$$\|(\mathbf{A}(\rho))^{-1}\| \leqslant C, \tag{65}$$

where $C > 0$ is a constant only depending on the a priori data $\mathcal{A}$ and N.

To prove (65), we shall write

$$\mathbf{A}(\rho) = \mathbf{A}(\rho_0) - \mathbf{P}, \tag{66}$$

where the inverse of $\mathbf{A}(\rho_0)$ is given explicitly in (50), and $\mathbf{P} = \mathbf{P}(\rho)$ is a perturbation due to the change of mass $r_\epsilon(x)$. Denoting $\Delta v_k(x) = v_k(x;\rho) - v_k(x;\rho_0) \equiv v_k(x;\rho) - v_k(x)$, for every $n,k = 1,\dots N$, by (60) we have

$$\begin{aligned} -P_{nk} = {} & 2\int_0^{\frac{L}{2}} \left(v_k v_n^2 \Delta v_k + v_n v_k^2 \Delta v_n\right) + \int_0^{\frac{L}{2}} \left(v_n^2(\Delta v_k)^2 + v_k^2(\Delta v_n)^2 + 4 v_n v_k \Delta v_n \Delta v_k\right) \\ & + 2\int_0^{\frac{L}{2}} \left(v_n \Delta v_n (\Delta v_k)^2 + v_k \Delta v_k (\Delta v_n)^2\right) + \int_0^{\frac{L}{2}} (\Delta v_n)^2 (\Delta v_k)^2. \end{aligned} \tag{67}$$

In order to simplify the analysis, we shall control the L^∞ norm of all the quantities inside the integrals in (67). The norm $\|v_k\|_\infty$ (even in the whole interval $(0,L)$) can be bound via inequality (37), which holds for unperturbed eigenfunctions with a constant $C > 0$ only depending on the a priori data $\mathcal{A}$. In order to bound $\|\Delta v_k\|_\infty$, we use the Rellich-Kondrachov's Theorem (see [40], Theorem *IX*.26) and estimate (157): for every $k \geqslant 1$ we have

$$\|\Delta v_k\|_{L^\infty(0,L)} \leqslant C\|\Delta v_k\|_{H^2(0,L)} \leqslant C\|\rho - \rho_0\|^{\frac{1}{2}}_{L^2(0,L)} \leqslant C\epsilon^{\frac{1}{2}}, \tag{68}$$

for every $\epsilon \leqslant \widehat{\epsilon}(< 1)$, where $\widehat{\epsilon}$ has been introduced in Theorem 3.1, and $C > 0$ is a constant only depending on the a priori data $\mathcal{A}$ and k. Therefore, for every $n,k = 1,\dots,N$ and for every ϵ such that $\epsilon \leqslant \widehat{\epsilon}$, we have

$$|P_{nk}| \leqslant C\left(\epsilon^{\frac{1}{2}} + \epsilon + \epsilon^{\frac{3}{2}} + \epsilon^2\right) \leqslant C\epsilon^{\frac{1}{2}} \tag{69}$$

and

$$\|\mathbf{P}\| \leqslant C_P \epsilon^{\frac{1}{2}}, \tag{70}$$

where $C_P > 0$ is a constant only depending on the a priori data $\mathcal{A}$ and N.

Let us introduce the number

$$\widehat{\epsilon}_\rho = \min\left\{\widehat{\epsilon}, \left(\frac{1}{2C_P\|(\mathbf{A}(\rho_0))^{-1}\|}\right)^2\right\}. \tag{71}$$

Note that, possibly increasing C_P, the number $\left(\frac{1}{2C_P\|(\mathbf{A}(\rho_0))^{-1}\|}\right)^2$ is less than 1. We now prove that if $\mathbf{P}$ satisfies (70) for every $\epsilon \leqslant \widehat{\epsilon}_\rho$, then $\mathbf{A}(\rho)$ is nonsingular, and

$$\|(\mathbf{A}(\rho))^{-1}\| \leqslant \frac{\|(\mathbf{A}(\rho_0))^{-1}\| \cdot \|\mathbf{I}\|}{1 - \|(\mathbf{A}(\rho_0))^{-1}\| \cdot \|\mathbf{P}\|}, \tag{72}$$

where $\mathbf{I}$ is the identity matrix in $\mathbb{R}^{N\times N}$. Let $\mathbf{x} \in \mathbb{R}^N \setminus \{\mathbf{0}\}$. Then, since $\mathbf{A}(\rho_0)$ is nonsingular, it is enough to prove that $\left(\mathbf{I} - (\mathbf{A}(\rho_0))^{-1}\mathbf{P}\right)\mathbf{x} \neq \mathbf{0}$ for every $\mathbf{x} \in \mathbb{R}^N \setminus \{\mathbf{0}\}$. We have

$$\|\left(\mathbf{I} - (\mathbf{A}(\rho_0))^{-1}\mathbf{P}\right)\mathbf{x}\| \geqslant \left(1 - \|(\mathbf{A}(\rho_0))^{-1}\| \cdot \|\mathbf{P}\|\right)\|\mathbf{x}\| > 0, \tag{73}$$

since, by (70) and (71), for every $\epsilon, 0 < \epsilon \leqslant \widehat{\epsilon}_\rho$,

$$1 - \|(\mathbf{A}(\rho_0))^{-1}\| \cdot \|\mathbf{P}\| \geqslant 1 - \|(\mathbf{A}(\rho_0))^{-1}\| C_P \epsilon^{\frac{1}{2}} \geqslant \frac{1}{2} > 0. \tag{74}$$

Hence, if $\mathbf{x} \neq \mathbf{0}$, $\left(\mathbf{I} - (\mathbf{A}(\rho_0))^{-1}\mathbf{P}\right)\mathbf{x} \neq \mathbf{0}$ or, equivalently, $(\mathbf{A}(\rho_0) - \mathbf{P})\mathbf{x} \neq \mathbf{0}$ and $\mathbf{A}(\rho) = \mathbf{A}(\rho_0) - \mathbf{P}$ is nonsingular.

Now, from the identity $(\mathbf{A}(\rho_0) - \mathbf{P})(\mathbf{A}(\rho_0) - \mathbf{P})^{-1} = \mathbf{I}$, it follows that

$$\left(\mathbf{I} - (\mathbf{A}(\rho_0))^{-1}\mathbf{P}\right)^{-1} = \mathbf{I} + (\mathbf{A}(\rho_0))^{-1}\mathbf{P}\left(\mathbf{I} - (\mathbf{A}(\rho_0))^{-1}\mathbf{P}\right)^{-1} \tag{75}$$

and, then,

$$\|\left(\mathbf{I} - (\mathbf{A}(\rho_0))^{-1}\mathbf{P}\right)^{-1}\| \leqslant \frac{\|\mathbf{I}\|}{1 - \|(\mathbf{A}(\rho_0))^{-1}\| \cdot \|\mathbf{P}\|}. \tag{76}$$

Inequalities (76) and (72) are equivalent, and imply (65).

Step ii). In order to control $|\delta\lambda^{(i)}|$, we follow the steps of the iterative procedure shown in Section 3.3.

At step ♯1, we use the fundamental identity (31) between the unperturbed 0th state (corresponding to $\rho^{(0)}(x) = \rho_0$) and the state to be identified (corresponding to the unknown mass coefficient, say $\overline{\rho}(x)$, and target eigenvalues $\{\lambda_n^{exp}\}, n = 1, \ldots, N$):

$$\lambda_n^{exp} = \lambda_n(\rho^{(0)}) - \lambda_n(\rho^{(0)})\left\langle \Delta M^{(0)} v_n(\rho^{(0)}), v_n(\rho^{(0)})\right\rangle + \widetilde{O}_n(\mathrm{EXP} - (0)), \tag{77}$$

$n = 1, \ldots, N$, where $\Delta M^{(0)} = \overline{\rho}(x) - \rho^{(0)}(x)$ and the higher order term $\widetilde{O}_n(\mathrm{EXP} - (0))$ depends on the initial state $\rho^{(0)}$ and on the variations $\Delta M^{(0)}, \Delta\lambda_n^{(0)} = \lambda_n^{exp} - \lambda_n(\rho^{(0)}), \Delta v_n(x) = v_n(x;\overline{\rho}) - v_n(x;\rho^{(0)})$. The mass coefficient $\rho^{(0)}$ is updated at step ♯1 as

$$\rho^{(1)}(x) = \rho^{(0)}(x) + r^{(0)}(x), \tag{78}$$

where $r^{(0)}(x)$ (given in (54) for $j = 0$) is determined by neglecting the term $\widetilde{O}_n(\mathrm{EXP} - (0))$ in (77), e.g., for every $n = 1, \ldots, N$,

$$\lambda_n^{exp} - \lambda_n(\rho^{(0)}) = -\lambda_n(\rho^{(0)})\langle r^{(0)} v_n(\rho^{(0)}), v_n(\rho^{(0)})\rangle. \tag{79}$$

By using the updated value of the mass coefficient $\rho^{(1)}(x)$, we now estimate $\lambda_n(\rho^{(1)}), n = 1, \ldots, N$. By applying the fundamental identity (31) between the states $\rho^{(0)}(x)$ and $\rho^{(1)}(x)$, we have

$$\lambda_n(\rho^{(1)}) - \lambda_n(\rho^{(0)}) = -\lambda_n(\rho^{(0)})\langle r^{(0)} v_n(\rho^{(0)}), v_n(\rho^{(0)})\rangle + \widetilde{O}_n((1) - (0)). \tag{80}$$

The first term on the right hand side of (80) can be determined by (79), namely

$$\lambda_n(\rho^{(1)}) - \lambda_n(\rho^{(0)}) = \lambda_n^{exp} - \lambda_n(\rho^{(0)}) + \widetilde{O}_n((1) - (0)), \tag{81}$$

that is

$$\lambda_n(\rho^{(1)}) - \lambda_n^{exp} = \widetilde{O}_n((1) - (0)), \quad n = 1, \ldots, N. \tag{82}$$

Similarly, at step ♯2, the mass coefficient is updated as

$$\rho^{(2)}(x) = \rho^{(1)}(x) + r^{(1)}(x), \tag{83}$$

where $r^{(1)}(x)$ satisfies

$$\lambda_n^{exp} - \lambda_n\big(\rho^{(1)}\big) = -\lambda_n\big(\rho^{(1)}\big)\big\langle r^{(1)} v_n\big(\rho^{(1)}\big), v_n\big(\rho^{(1)}\big)\big\rangle, \tag{84}$$

$n = 1, \dots, N$. The identity (31) between the states $\rho^{(1)}(x)$ and $\rho^{(2)}(x)$ reads as

$$\lambda_n\big(\rho^{(2)}\big) - \lambda_n\big(\rho^{(1)}\big) = -\lambda_n\big(\rho^{(1)}\big)\big\langle r^{(1)} v_n\big(\rho^{(1)}\big), v_n\big(\rho^{(1)}\big)\big\rangle + \widetilde{O}_n((2) - (1)), \tag{85}$$

and, by (84) and (85), we obtain

$$\lambda_n\big(\rho^{(2)}\big) - \lambda_n^{exp} = \widetilde{O}_n((2) - (1)), \quad n = 1, \dots, N. \tag{86}$$

By iteration, at step $\sharp(i+1)$ we have

$$\lambda_n\big(\rho^{(i+1)}\big) - \lambda_n^{exp} = \widetilde{O}_n((i+1) - (i)), \quad n = 1, \dots, N. \tag{87}$$

At this point we need to bound the high order term $\widetilde{O}_n((i+1) - (i))$ appearing in (87).

Let us first estimate $\widetilde{O}_n((1) - (0))$. By (31) (written between the unperturbed state $\rho^{(0)}$ and the first updated state $\rho^{(1)}$) we have

$$\begin{aligned} |\widetilde{O}_n((1) - (0))| &\leqslant \lambda_n |\langle \Delta M(\Delta v_n), v_n\rangle| + |\Delta\lambda_n| \cdot |\langle M(\Delta v_n), v_n\rangle| + |\Delta\lambda_n| \cdot |\langle \Delta M(v_n), v_n\rangle| + |\Delta\lambda_n| \cdot |\langle \Delta M(\Delta v_n), v_n\rangle| \\ &\equiv A_n + B_n + C_n + D_n. \end{aligned} \tag{88}$$

Let us consider the term A_n. By using Hölder inequality, we have

$$A_n \leqslant \lambda_n ||v_n||_\infty \int_0^L |\Delta M(x)| \cdot |v_n(x; \rho^{(1)}) - v_n(x; \rho^{(0)})| dx \leqslant \lambda_n ||v_n||_\infty ||\Delta M||_2 \cdot ||v_n(x; \rho^{(1)}) - v_n(x)||_2. \tag{89}$$

Recalling that $\Delta M = r^{(0)}(x) = \sum_{k=1}^N \beta_k^{(0)} \Phi_k(x; \rho^{(0)}) \chi_{\left[0, \frac{L}{2}\right]}$, with $\Phi_k(x; \rho^{(0)}) = v_k^2(x; \rho^{(0)})$, and noticing that $\|v_n\|_\infty$ can be estimated via (37), we have

$$||\Delta M||_2 \leqslant \frac{L^{\frac{3}{2}}}{a} \Lambda |\beta^{(0)}|, \tag{90}$$

where the quantity

$$\Lambda^{(0)} = \left(\sum_{k=1}^N \lambda_k^2 \right)^{\frac{1}{2}} \tag{91}$$

can be calculated in terms of the unperturbed nanorod and, therefore, it depends on the a priori data set $\mathcal{A}$ only. By using (37), (90) and (35) in (89), we have

$$A_n \leqslant (\lambda_n)^{\frac{3}{2}} L \left(\frac{L}{a}\right)^{\frac{5}{2}} \left(\Lambda^{(0)}\right)^2 C_n^v |\beta^{(0)}|^2. \tag{92}$$

The other terms in (88) can be evaluated similarly, namely

$$B_n \leqslant \rho_0^{\frac{1}{2}} L \left(\frac{L}{a}\right)^2 \left(\Lambda^{(0)}\right)^2 C_n^\lambda C_n^v |\beta^{(0)}|^2, \tag{93}$$

$$C_n \leqslant \lambda_n L^{\frac{3}{2}} \left(\frac{L}{a}\right)^3 \left(\Lambda^{(0)}\right)^2 C_n^\lambda |\beta^{(0)}|^2, \tag{94}$$

$$D_n \leqslant (\lambda_n)^{\frac{1}{2}} L^{\frac{3}{2}} \left(\frac{L}{a}\right)^{\frac{7}{2}} \left(\Lambda^{(0)}\right)^3 C_n^\lambda C_n^v |\beta^{(0)}|^3. \tag{95}$$

Therefore, collecting the estimates (92)–(95), we have

$$|\widetilde{O}_n((1) - (0))| \leqslant C|\beta^{(0)}|^2 \left(1 + C|\beta^{(0)}|\right), \tag{96}$$

where $C > 0$ is a constant only depending on the a priori data $\mathcal{A}$ and $n, n = 1, \dots, N$. By using (65) in (56) (for $j = 0$), we have

$$|\beta^{(0)}| \leqslant C|\delta\lambda^{(0)}|, \tag{97}$$

and (96) becomes

$$|\widetilde{O}_n((1)-(0))| \leqslant C|\delta\lambda^{(0)}|^2\left(1+C|\delta\lambda^{(0)}|\right) \leqslant C|\delta\lambda^{(0)}|^2, \tag{98}$$

provided that $|\delta\lambda^{(0)}| \leqslant 1$, where $C>0$ is a constant only depending on the a priori data $\mathcal{A}$ and n. Therefore, using (98) in (82), for every $n=1,\dots,N$, we have

$$|\lambda_n(\rho^{(1)}) - \lambda_n^{exp}| \leqslant C|\delta\lambda^{(0)}|^2, \tag{99}$$

for $|\delta\lambda^{(0)}| \leqslant 1$, where $C>0$ is a constant only depending on the a priori data $\mathcal{A}$ and n.

We proceed similarly in estimating $\widetilde{O}_n((2)-(1))$. By adapting the previous analysis to the states $\rho^{(2)}$ and $\rho^{(1)}$, we obtain

$$|\widetilde{O}_n((2)-(1))| \leqslant C|\beta^{(1)}|^2\left(1+C|\beta^{(1)}|\right), \tag{100}$$

and, recalling (65) and (56),

$$|\widetilde{O}_n((2)-(1))| \leqslant C|\delta\lambda^{(1)}|^2, \tag{101}$$

that is, by (86),

$$|\lambda_n(\rho^{(2)}) - \lambda_n^{exp}| \leqslant C|\delta\lambda^{(1)}|^2, \tag{102}$$

for $|\delta\lambda^{(1)}| \leqslant 1$, where $C>0$ is a constant only depending on the a priori data $\mathcal{A}$ and n. Using (99) in (102) (and noticing that $\lambda_n(\rho^{(1)})$ can be estimated from below by a positive quantity only depending on the a priori data $\mathcal{A}$ and n), we have

$$|\lambda_n(\rho^{(2)}) - \lambda_n^{exp}| \leqslant C|\delta\lambda^{(0)}|^{2\cdot 2}. \tag{103}$$

By iteration, for every $i \geqslant 1$ and $n=1,\dots,N$, we obtain

$$|\lambda_n(\rho^{(i)}) - \lambda_n^{exp}| \leqslant C|\delta\lambda^{(0)}|^{2^i}, \tag{104}$$

where $C>0$ is a constant only depending on the a priori data $\mathcal{A}$ and n, and $|\delta\lambda^{(0)}| \leqslant 1$.

Conclusion of the proof. By using the estimates (65) and (104), the series $\sum_{i=0}^{\infty} r^{(i)}(x)$ in (64) is L^2-uniformly convergent to a continuous function in $\left[0,\frac{L}{2}\right]$, since the ith term can be bounded as

$$\|r^{(i)}(x)\|_{L^2\left[0,\frac{L}{2}\right]} \leqslant C|\delta\lambda^{(0)}|^{2^i}, \quad i \geqslant 0, \tag{105}$$

where $C>0$ is a constant only depending on the a priori data $\mathcal{A}$, and the numerical series $\sum_{i=0}^{\infty}|\delta\lambda^{(0)}|^{2^i}$ is convergent provided that $|\delta\lambda^{(0)}| \leqslant \widehat{\epsilon}_\lambda < 1$ (Weierstrass's criterion).

Summarizing, in this section we have proved the following result:

If $\epsilon \leqslant \widehat{\epsilon}_\rho$, where $\widehat{\epsilon}_\rho$ is given in (71), and $|\delta\lambda^{(0)}| \leqslant \widehat{\epsilon}_\lambda < 1$, then the iterative procedure of identification converges uniformly to a continuous function in $\left[0,\frac{L}{2}\right]$.

Our convergence result has local character, since the proof is built on the assumption that the mass variation is a small perturbation of the total mass of the unperturbed nanorod. It would be interesting, and also useful for practical applications, to determine or, at least, to find good approximation of the maximum value allowed for $\widehat{\epsilon}_\rho$. Moreover, the local character is also reflected on the condition $\widehat{\epsilon}_\lambda < 1$, which means that the first N eigenvalues of the unperturbed nanorod must be close enough to the corresponding target eigenvalues.

5. Application of the Generalized Fourier Coefficient method

5.1. Specimen

In order to illustrate the application of the identification method, reference is made to the geometrical and material properties of the nanorod used in [43]. In particular, the diameter D of the circular equivalent cross-section is equal to 100 μm ($=100\cdot 10^{-6}$ m) and the length L is taken equal to $20D$; the material length scale parameters are assumed to be equal, and $\ell_0=\ell_1=\ell_2=\ell=17.6$ μm; the Young's modulus E is equal to 1.44 GPa; the Poisson's coefficient is $\nu=0.38$; and the volume mass density is equal to $\rho_{vol}=1000$ kg/m^3. The coefficients a, b, ρ_0 corresponding to the above parameters take the value $a=11.310$ $N, b=3.554\cdot 10^{-9}$ Nm^2, $\rho_0=\rho_{vol}\cdot\pi\frac{D^2}{4}=7.854\cdot 10^{-6}$ kg/m, respectively.

5.2. Discrete model and eigenvalue problem

The practical application of the mass identification method requires the development of a specific numerical code. The weak formulation of the eigenvalue problem (15)–(17) consists in determining a non-trivial function $v \in \mathcal{H}$ (see definition (24)), and a positive real number λ such that

$$\int_0^L (b v'' \varphi'' + a v' \varphi') = \lambda \int_0^L \rho v \varphi, \tag{106}$$

for every $\varphi \in \mathcal{H}$. To find a finite element model of the weak formulation (106), we work on the finite-dimensional subspace of $\mathcal{H}$ formed by three-degree polynomial spline approximation of the axial displacement of the nanorod in each element. More precisely, let $\{x_0 = 0 < x_1 < x_2 < \ldots < x_{N_e} = L\}$ be the nodes of a mesh of the interval $[0, L]$, with $x_{i+1} - x_i = \Delta x = \frac{L}{N_e}$, for every $i = 0, 1, \ldots, N_e$. Therefore, the discrete version of (106) consists in finding the approximating eigenpair $\left(\widetilde{\lambda}, \widetilde{\mathbf{v}}\right)$, $\widetilde{\mathbf{v}} \in \mathbb{R}^{2N_e} \setminus \{\mathbf{0}\}$, solution to

$$\widetilde{\mathbf{F}}\widetilde{\mathbf{v}} = \widetilde{\lambda}\widetilde{\mathbf{M}}\widetilde{\mathbf{v}}, \tag{107}$$

where $\widetilde{\mathbf{F}}, \widetilde{\mathbf{M}}$ is the $2N_e \times 2N_e$ real symmetric matrix of the stiffness and of the inertia of the nanorod, respectively.

The mass coefficient $\rho = \rho(x)$ is approximated by a continuous piecewise-linear function, that is, $\widetilde{\rho}(x) = \rho(x_i) + \{(\rho(x_{i+1}) - \rho(x_i))/(\Delta x)\}x$ for $x \in [x_i, x_{i+1}]$. Therefore, the (n, k) entry of the local mass, $\left(\widetilde{M}_i^{nk}\right)$, and stiffness, $\left(\widetilde{F}_i^{nk}\right)$, matrix are given by

$$\widetilde{M}_i^{nk} = \int_{x_i}^{x_{i+1}} \widetilde{\rho}(x)\varphi_n(x)\varphi_k(x)dx, \;\; \widetilde{F}_i^{nk} = \int_{x_i}^{x_{i+1}} \left(b\varphi_n''(x)\varphi_k''(x) + a\varphi_n'(x)\varphi_k'(x)\right)dx, \tag{108}$$

$n, k = 1, \ldots, 4$, and are evaluated in exact form. Numerical integration of the quantities (60) was developed by means of a standard trapezoidal method. The discrete eigenvalue problem (107) was solved by using the Implicit Restarted Lanczos's method [44]. The identification procedure was built in Scilab environment (version 5.5.2) by developing a specific numerical code. Regarding the computational burden, the time needed to complete a single iteration of the identification algorithm (for $N_e = 200$) was about 1 s.

5.3. Results

In this section we present a selection of the results obtained in an extended series of applications of the Generalized Fourier Coefficient Method. Among other parameters, the procedure has been tested with respect to the number N of the first eigenfrequencies used and to the geometry of the mass variation (e.g., position, intensity, regularity). In particular, the efficiency of the method has been evaluated on two main classes of mass variations corresponding to *smooth* (Section 5.3.1) or *discontinuous* (Section 5.3.2) function r_ϵ. In both cases, the support of the mass variation coincides with an interval contained in $(0, \frac{L}{2})$. We have first considered free-error data, i.e., the measurement errors are null with the exception of the errors induced by the numerical approximation via the finite element method. The analysis of *overlapping* mass variations, possibly having disconnected support, is considered in Section 5.3.3. Section 5.3.4 is devoted to the application of suitable physical filtering to improve the accuracy of identification. Finally, the stability of the reconstruction in presence of noise is investigated in Section 5.3.5.

5.3.1. Identification of smooth mass densities

In this series of simulations, the mass density of the perturbed nanorod is defined as

$$\rho(x) = \rho_0 + \rho_0 t \cos^2\left(\frac{\pi(x - s)}{c}\right)\chi_{\left[s-\frac{c}{2}, s+\frac{c}{2}\right]}, \tag{109}$$

where s is the central point of the support of the mass variation, c is the length of the support, $\rho_0 t$ is the maximum amplitude of variation, see Fig. 1(a). Note that $\rho \in C^1[0, L]$.

The definition (109) allows to consider a wide family of coefficients, including either localized or diffuse mass variations. In the sequel, reference is made mainly to positions $\frac{s}{L} = 0.15,\ 0.25,\ 0.35$, extensions $\frac{c}{L} = 0.10,\ 0.20,\ 0.30$, and intensities $t = 0.10,\ 0.20,\ 0.50,\ 1.00$, for all the possible combinations of the parameters. Therefore, the global mass change ranges from 0.5 percent to 15 percent of the initial mass $\rho_0 L$, for $\left(\frac{c}{L} = 0.10,\ t = 0.10\right)$ and $\left(\frac{c}{L} = 0.30,\ t = 1.0\right)$, respectively.

In order to select a suitable mesh for the numerical solution of the eigenvalue problem, preliminary tests have been carried out on the uniform nanorod, for which analytical closed form expressions of the eigenpairs are available. The analysis suggests to assume a mesh with $N_e = 200$ equally spaced finite elements, which turns out to be a good compromise between accuracy (maximum error on the first 15 eigenvalues less than 10^{-4} percent) and computational cost for all the cases studied,

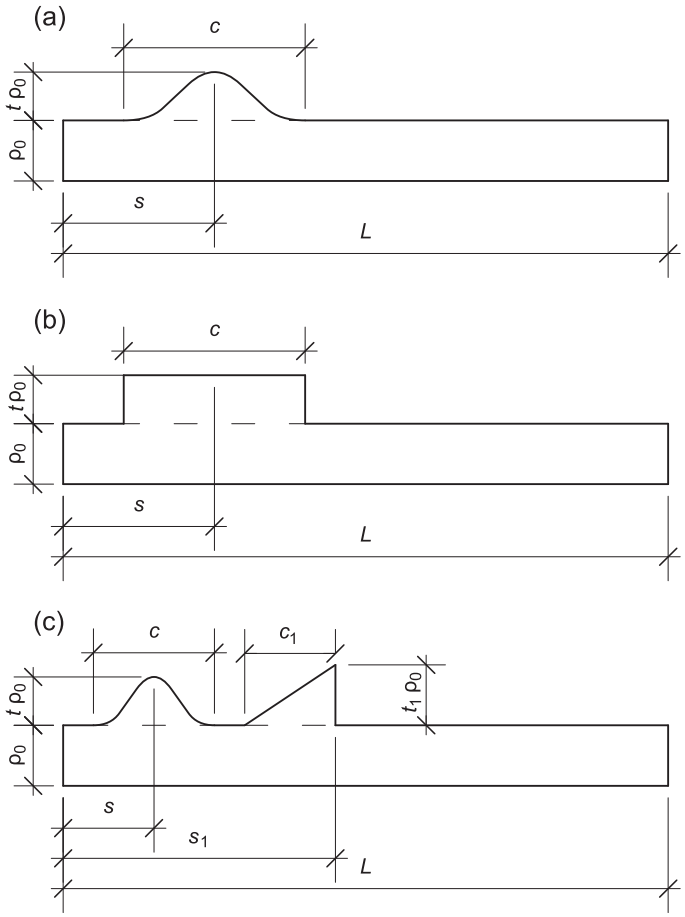

Fig. 1. Mass density per unit length $\rho = \rho(x)$ to be identified in $[0, \frac{L}{2}]$. (a) Smooth mass changes as in (109); (b) discontinuous mass changes as in (110); (c) overlapping mass changes as in (111).

including the reconstruction procedure, see Table 1. Moreover, this set of preliminary tests suggests to choose $\gamma = 10^{-5}$ in the stopping criterion (63).

Regarding the influence of the number N of eigenvalue data, here we will focus on the most two challenging cases. The first one ($\frac{s}{L} = 0.35, \frac{c}{L} = 0.1, t = 0.1$), see Fig. 2, corresponds to small mass increase located in a small interval, which allows to assess the sensitivity of the method to the identification of the mass perturbation just as it occurs in the nanorod. The second case ($\frac{s}{L} = 0.35, \frac{c}{L} = 0.1, t = 1$, see Fig. 3) deals with mass variation having the same support as before, but with an abrupt increase of mass with large L^∞ amplitude.

The analysis of Fig. 2 shows that the identified coefficient agrees well with the exact one, and accuracy of reconstruction rapidly improves as N increases. Similar properties can be deduced from the analysis of Fig. 3, apart from the oscillatory character of the reconstructed coefficient, which is now more evident for $N = 6, 9$, whereas it becomes almost negligible when $N = 15$.

For the sake of completeness, it should be noted that part of our results involve not necessarily small mass variations, see, for example, Fig. 4. This would suggest that the proposed reconstruction method has some unexpected potential, in spite of the fact that the proof of convergence presented in Section 4 requires to work in a sufficiently small neighborhood of the referential nanorod.

Finally, some synthetic numerical information concerning the sequence of iterations is reported in Table 2. Few iterations are sufficient to satisfy the convergence criterion, e.g., less than five in these cases. The quantity e defined in (63), which can be considered at each iteration step as the average discrepancy between identified and target eigenvalues, is reduced by at least $3 - 4$ orders of magnitude with respect to the initial value. The errors on the mass coefficient, either evaluated on L^2 or L^∞ norm, are reduced significantly through the iterations, albeit to a lesser extent than e. In particular, the relative error in L^∞ norm is even more than one order of magnitude less than the initial value, so confirming the accuracy of the reconstruction of regular mass variations. It should also be noted that the matrix $\mathbf{A}^{(j)}$ remains well conditioned during the iterations, with

Table 1
First 25 eigenvalues of the clamped–clamped uniform unperturbed nanorod in (1)–(3), with physical parameters as in Section 5.1. Comparison between analytical (λ_n, column 2) and numerical (λ_n^{FEM}) values obtained with $N_e = 100, 200, 400$ equally spaced finite elements. Percentage errors: $e_n = 100 \times (\lambda_n^{FEM} - \lambda_n)/\lambda_n$ for $N_e = 100$ (column 3), $N_e = 200$ (column 4), $N_e = 400$ (column 5).

n	λ_n $(\mathrm{rad/s})^2$	$N_e = 100$	$N_e = 200$	$N_e = 400$
1	$3.556 \cdot 10^{+12}$	$1.4 \cdot 10^{-6}$	$1.4 \cdot 10^{-6}$	$1.4 \cdot 10^{-6}$
2	$1.426 \cdot 10^{+13}$	$1.4 \cdot 10^{-6}$	$1.4 \cdot 10^{-6}$	$1.4 \cdot 10^{-6}$
3	$3.220 \cdot 10^{+13}$	$1.5 \cdot 10^{-6}$	$1.5 \cdot 10^{-6}$	$1.5 \cdot 10^{-6}$
4	$5.755 \cdot 10^{+13}$	$5.0 \cdot 10^{-7}$	$5.0 \cdot 10^{-7}$	$5.0 \cdot 10^{-7}$
5	$9.055 \cdot 10^{+13}$	$1.6 \cdot 10^{-6}$	$5.2 \cdot 10^{-7}$	$5.2 \cdot 10^{-7}$
6	$1.315 \cdot 10^{+14}$	$8.1 \cdot 10^{-6}$	$5.2 \cdot 10^{-7}$	$5.2 \cdot 10^{-7}$
7	$1.807 \cdot 10^{+14}$	$1.3 \cdot 10^{-5}$	$2.4 \cdot 10^{-6}$	$2.4 \cdot 10^{-6}$
8	$2.387 \cdot 10^{+14}$	$2.6 \cdot 10^{-5}$	$1.2 \cdot 10^{-6}$	$1.2 \cdot 10^{-6}$
9	$3.059 \cdot 10^{+14}$	$5.3 \cdot 10^{-5}$	$3.9 \cdot 10^{-6}$	$6.6 \cdot 10^{-7}$
10	$3.829 \cdot 10^{+14}$	$9.9 \cdot 10^{-5}$	$4.9 \cdot 10^{-6}$	$-2.8 \cdot 10^{-7}$
11	$4.703 \cdot 10^{+14}$	$1.7 \cdot 10^{-4}$	$1.1 \cdot 10^{-5}$	$2.6 \cdot 10^{-7}$
12	$5.688 \cdot 10^{+14}$	$2.9 \cdot 10^{-4}$	$1.7 \cdot 10^{-5}$	$1.3 \cdot 10^{-6}$
13	$6.792 \cdot 10^{+14}$	$4.6 \cdot 10^{-4}$	$2.7 \cdot 10^{-5}$	$2.5 \cdot 10^{-6}$
14	$8.022 \cdot 10^{+14}$	$7.0 \cdot 10^{-4}$	$4.4 \cdot 10^{-5}$	$2.4 \cdot 10^{-6}$
15	$9.389 \cdot 10^{+14}$	$1.0 \cdot 10^{-3}$	$6.4 \cdot 10^{-5}$	$3.9 \cdot 10^{-6}$
16	$1.090 \cdot 10^{+15}$	$1.5 \cdot 10^{-3}$	$9.1 \cdot 10^{-5}$	$8.2 \cdot 10^{-6}$
17	$1.257 \cdot 10^{+15}$	$2.1 \cdot 10^{-3}$	$1.3 \cdot 10^{-4}$	$9.6 \cdot 10^{-6}$
18	$1.440 \cdot 10^{+15}$	$2.9 \cdot 10^{-3}$	$1.8 \cdot 10^{-4}$	$1.4 \cdot 10^{-5}$
19	$1.642 \cdot 10^{+15}$	$3.9 \cdot 10^{-3}$	$2.4 \cdot 10^{-4}$	$1.5 \cdot 10^{-5}$
20	$1.862 \cdot 10^{+15}$	$5.2 \cdot 10^{-3}$	$3.2 \cdot 10^{-4}$	$2.0 \cdot 10^{-5}$
21	$2.103 \cdot 10^{+15}$	$6.8 \cdot 10^{-3}$	$4.2 \cdot 10^{-4}$	$2.4 \cdot 10^{-5}$
22	$2.365 \cdot 10^{+15}$	$8.8 \cdot 10^{-3}$	$5.4 \cdot 10^{-4}$	$3.2 \cdot 10^{-5}$
23	$2.651 \cdot 10^{+15}$	$1.1 \cdot 10^{-2}$	$6.9 \cdot 10^{-4}$	$4.2 \cdot 10^{-5}$
24	$2.961 \cdot 10^{+15}$	$1.4 \cdot 10^{-2}$	$8.7 \cdot 10^{-4}$	$5.6 \cdot 10^{-5}$
25	$3.297 \cdot 10^{+15}$	$1.7 \cdot 10^{-2}$	$1.1 \cdot 10^{-3}$	$6.7 \cdot 10^{-5}$

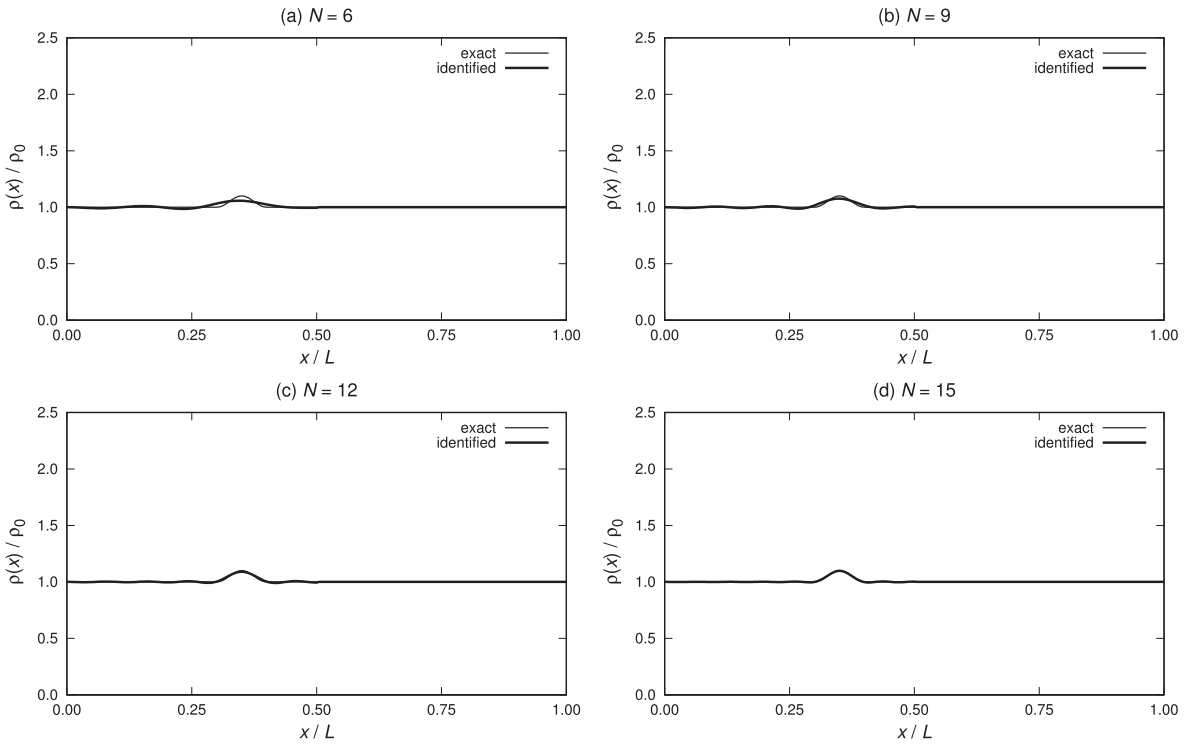

Fig. 2. Reconstruction of smooth mass changes as in (109), with $\frac{s}{L} = 0.35, \frac{\epsilon}{L} = 0.10$, $t = 0.10$, using the first $N = 6, 9, 12, 15$ eigenfrequencies.

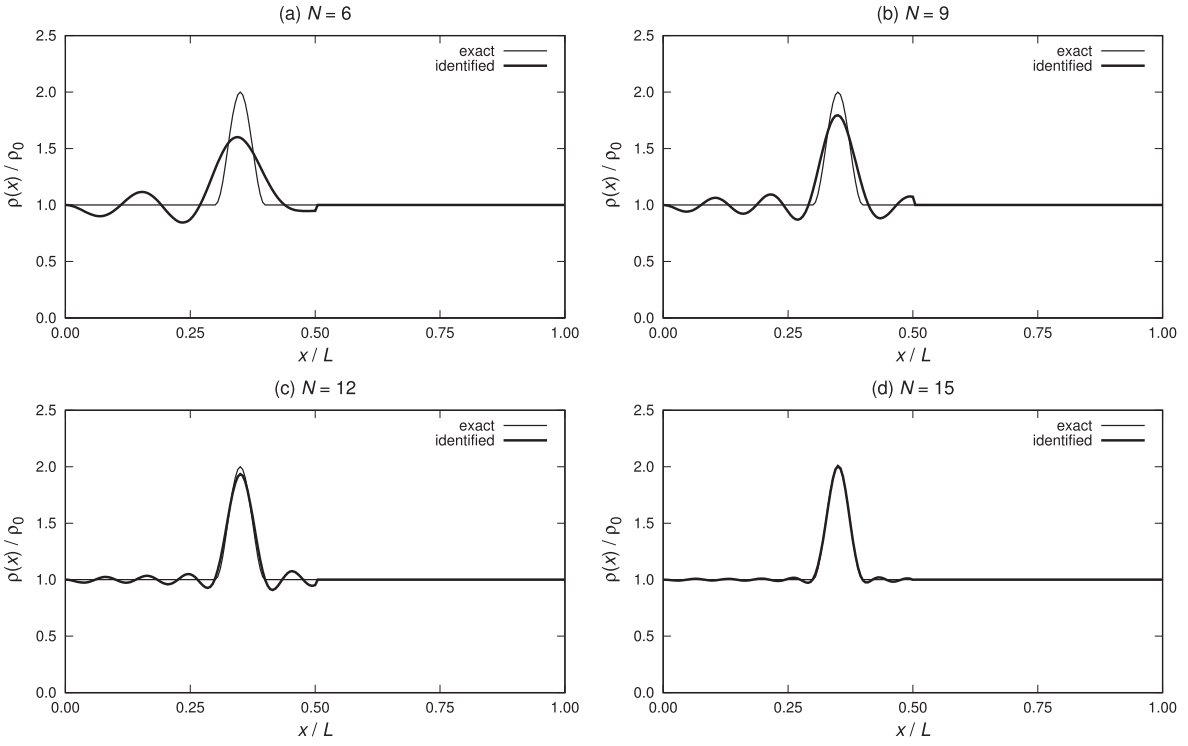

Fig. 3. Reconstruction of smooth mass changes as in (109), with $\frac{s}{L} = 0.35, \frac{c}{L} = 0.10$, $t = 1.00$, using the first $N = 6, 9, 12, 15$ eigenfrequencies.

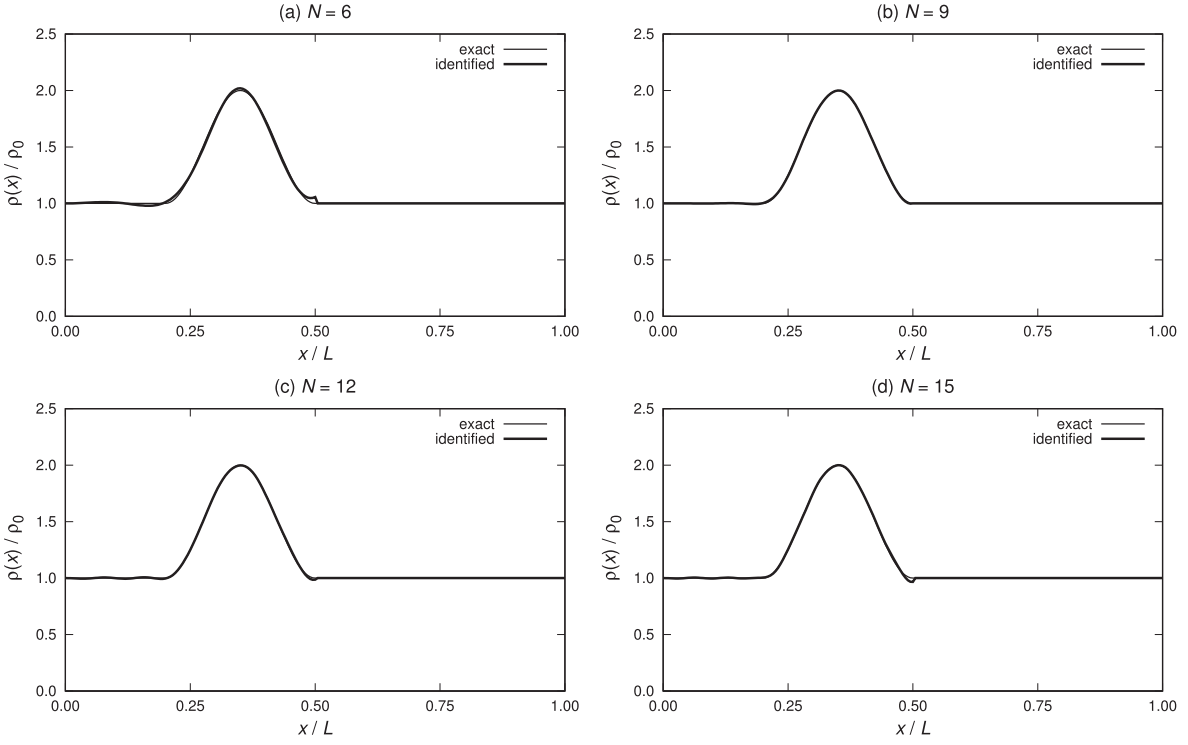

Fig. 4. Reconstruction of smooth mass changes as in (109), with $\frac{s}{L} = 0.35, \frac{c}{L} = 0.30$, $t = 1.00$, using the first $N = 6, 9, 12, 15$ eigenfrequencies.

condition number $\kappa\left(\mathbf{A}^{(j)}\right) = \|\mathbf{A}^{(j)}\| \, \|\left(\mathbf{A}^{(j)}\right)^{-1}\|$ ranging between 30 and 120 in all the cases studied. Here, $\|\mathbf{A}^{(j)}\| = \max_{|\mathbf{y}|=1} |\mathbf{A}^{(j)}\mathbf{y}|$, where $|\mathbf{y}| = \sqrt{\mathbf{y}\cdot\mathbf{y}}$ is the Euclidean norm of the vector $\mathbf{y} \in \mathbb{R}^N$.

5.3.2. Identification of discontinuous mass densities

The mass density to be determined is assumed equal to

Table 2
Some results of the reconstruction of smooth mass changes as in (109) versus iteration number j (up to convergence), with (a): $\frac{s}{L} = 0.35, \frac{c}{L} = 0.10, t = 0.10$ (Fig. 2); (b): $\frac{s}{L} = 0.35, \frac{c}{L} = 0.10, t = 1.00$ (Fig. 3); (c): $\frac{s}{L} = 0.35, \frac{c}{L} = 0.30, t = 1.00$ (Fig. 4), using the first $N = 6$ (columns $2-5$), $N = 15$ (columns $6-9$) eigenfrequencies. The quantity e is defined in (63); $e_{L^2} = \frac{\|\rho^{ident} - \rho^{exact}\|_{L^2}}{\|\rho^{exact}\|_{L^2}}$, $e_{L^\infty} = \frac{\|\rho^{ident} - \rho^{exact}\|_{L^\infty}}{\|\rho^{exact}\|_{L^\infty}}$, where $\rho^{ident} = \rho^{ident}(x)$, $\rho^{exact} = \rho^{exact}(x)$ are the identified and the exact mass density per unit length, respectively. $\kappa\left(\mathbf{A}^{(j)}\right)$ is the condition number of the matrix $\mathbf{A}^{(j)}$. The unperturbed nanorod corresponds to $j = 0$.

j	e	$\kappa\left(\mathbf{A}^{(j)}\right)$	e_{L^2}	e_{L^∞}	e	$\kappa\left(\mathbf{A}^{(j)}\right)$	e_{L^2}	e_{L^∞}
				(a)				
0	$2.40 \cdot 10^{-3}$	$1.30 \cdot 10^{+1}$	$1.92 \cdot 10^{-2}$	$9.09 \cdot 10^{-2}$	$1.44 \cdot 10^{-3}$	$3.10 \cdot 10^{+1}$	$1.92 \cdot 10^{-2}$	$9.09 \cdot 10^{-2}$
1	$3.11 \cdot 10^{-5}$	$1.31 \cdot 10^{+1}$	$1.04 \cdot 10^{-2}$	$3.95 \cdot 10^{-2}$	$3.84 \cdot 10^{-5}$	$3.12 \cdot 10^{+1}$	$1.58 \cdot 10^{-3}$	$5.34 \cdot 10^{-3}$
2	$5.12 \cdot 10^{-8}$	$1.41 \cdot 10^{+1}$	$1.04 \cdot 10^{-2}$	$3.88 \cdot 10^{-2}$	$3.35 \cdot 10^{-7}$	$3.64 \cdot 10^{+1}$	$1.31 \cdot 10^{-3}$	$4.43 \cdot 10^{-3}$
				(b)				
0	$2.33 \cdot 10^{-2}$	$1.30 \cdot 10^{+1}$	$1.81 \cdot 10^{-1}$	$5.00 \cdot 10^{-1}$	$1.29 \cdot 10^{-2}$	$3.10 \cdot 10^{+1}$	$1.81 \cdot 10^{-1}$	$5.00 \cdot 10^{-1}$
1	$2.52 \cdot 10^{-3}$	$1.31 \cdot 10^{+1}$	$1.00 \cdot 10^{-1}$	$2.43 \cdot 10^{-1}$	$2.23 \cdot 10^{-3}$	$3.12 \cdot 10^{+1}$	$5.70 \cdot 10^{-2}$	$1.47 \cdot 10^{-1}$
2	$9.00 \cdot 10^{-5}$	$2.36 \cdot 10^{+1}$	$9.68 \cdot 10^{-2}$	$2.02 \cdot 10^{-1}$	$2.63 \cdot 10^{-4}$	$8.16 \cdot 10^{+1}$	$1.14 \cdot 10^{-2}$	$2.55 \cdot 10^{-2}$
3	$3.37 \cdot 10^{-7}$	$2.60 \cdot 10^{+1}$	$9.68 \cdot 10^{-2}$	$2.02 \cdot 10^{-1}$	$7.77 \cdot 10^{-6}$	$1.14 \cdot 10^{+2}$	$7.17 \cdot 10^{-3}$	$1.50 \cdot 10^{-2}$
				(c)				
0	$6.42 \cdot 10^{-2}$	$1.30 \cdot 10^{+1}$	$2.82 \cdot 10^{-1}$	$5.00 \cdot 10^{-1}$	$3.64 \cdot 10^{-2}$	$3.10 \cdot 10^{+1}$	$2.82 \cdot 10^{-1}$	$5.00 \cdot 10^{-1}$
1	$1.24 \cdot 10^{-2}$	$1.31 \cdot 10^{+1}$	$9.46 \cdot 10^{-2}$	$1.74 \cdot 10^{-1}$	$7.03 \cdot 10^{-3}$	$3.12 \cdot 10^{+1}$	$9.57 \cdot 10^{-2}$	$1.84 \cdot 10^{-1}$
2	$9.08 \cdot 10^{-4}$	$2.44 \cdot 10^{+1}$	$1.53 \cdot 10^{-2}$	$3.54 \cdot 10^{-2}$	$6.14 \cdot 10^{-4}$	$5.89 \cdot 10^{+1}$	$1.44 \cdot 10^{-2}$	$3.08 \cdot 10^{-2}$
3	$2.20 \cdot 10^{-5}$	$3.25 \cdot 10^{+1}$	$9.97 \cdot 10^{-3}$	$2.79 \cdot 10^{-2}$	$1.54 \cdot 10^{-5}$	$7.92 \cdot 10^{+1}$	$4.64 \cdot 10^{-3}$	$1.78 \cdot 10^{-2}$
4	$4.89 \cdot 10^{-8}$	$3.30 \cdot 10^{+1}$	$9.96 \cdot 10^{-3}$	$2.80 \cdot 10^{-2}$	$9.11 \cdot 10^{-8}$	$8.11 \cdot 10^{+1}$	$4.62 \cdot 10^{-3}$	$1.75 \cdot 10^{-2}$

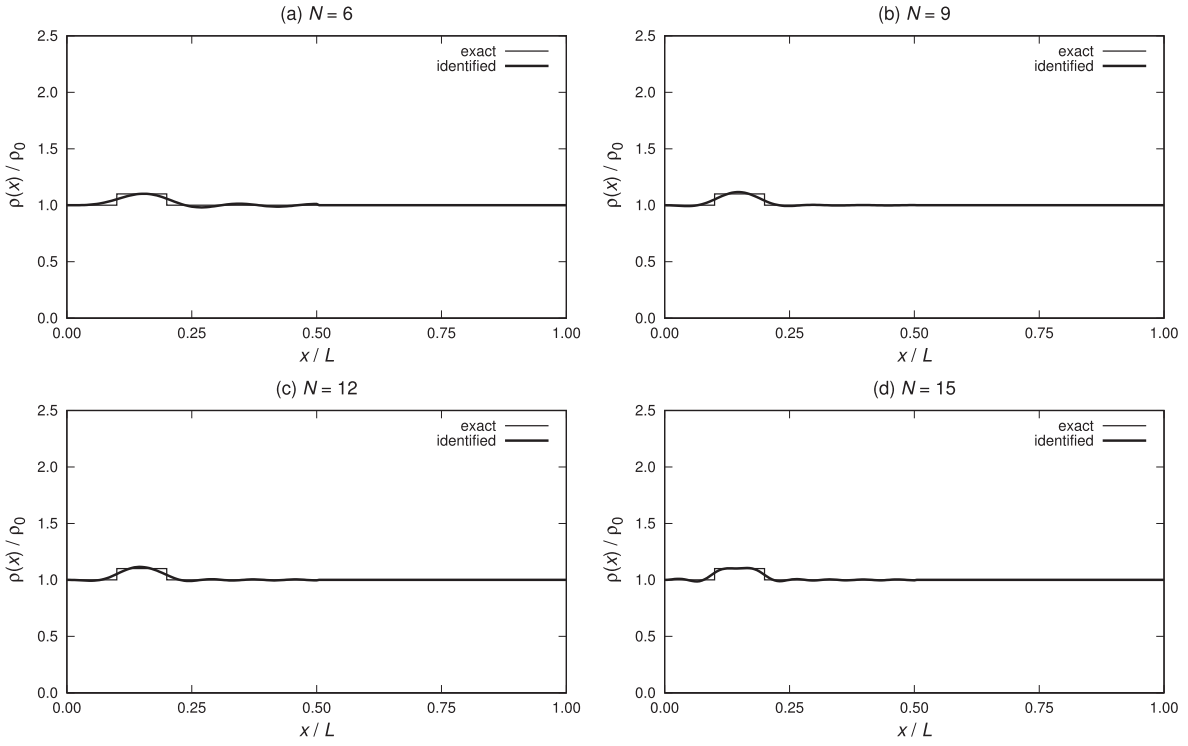

Fig. 5. Reconstruction of discontinuous mass changes as in (110), with $\frac{s}{L} = 0.15, \frac{c}{L} = 0.10$, $t = 0.10$, using the first $N = 6, 9, 12, 15$ eigenfrequencies.

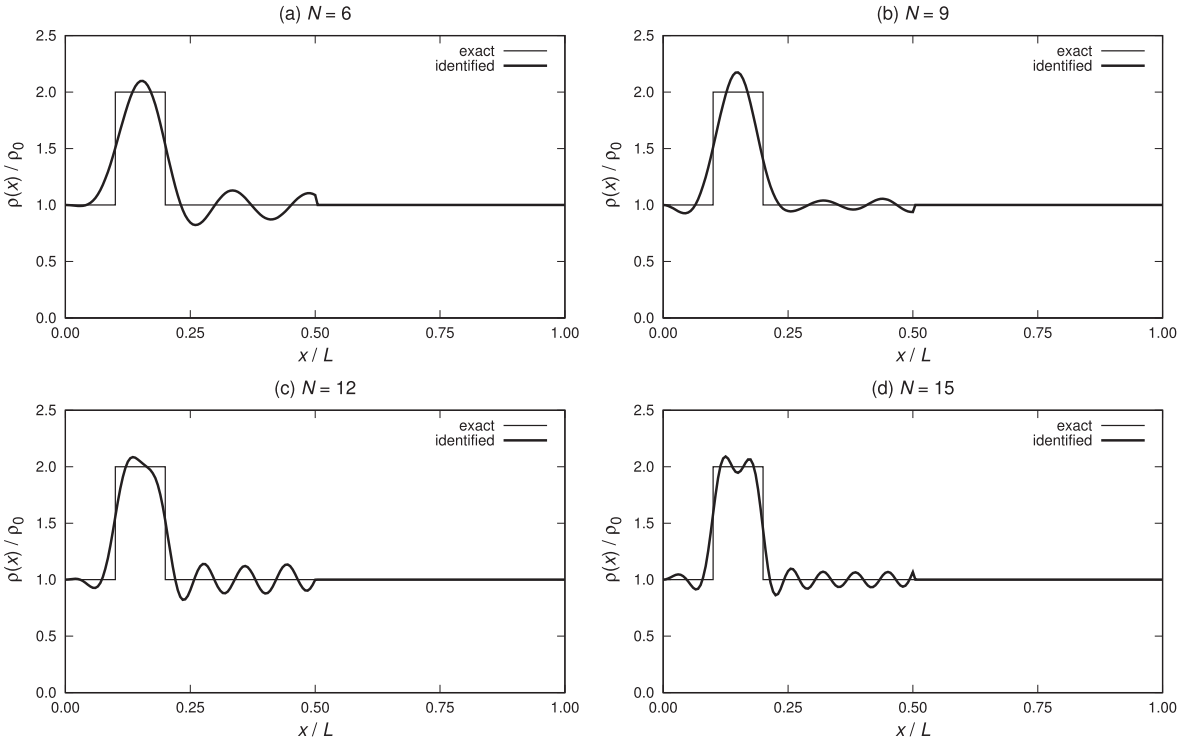

Fig. 6. Reconstruction of discontinuous mass changes as in (110), with $\frac{s}{L} = 0.15, \frac{\varepsilon}{L} = 0.10$, $t = 1.00$, using the first $N = 6, 9, 12, 15$ eigenfrequencies.

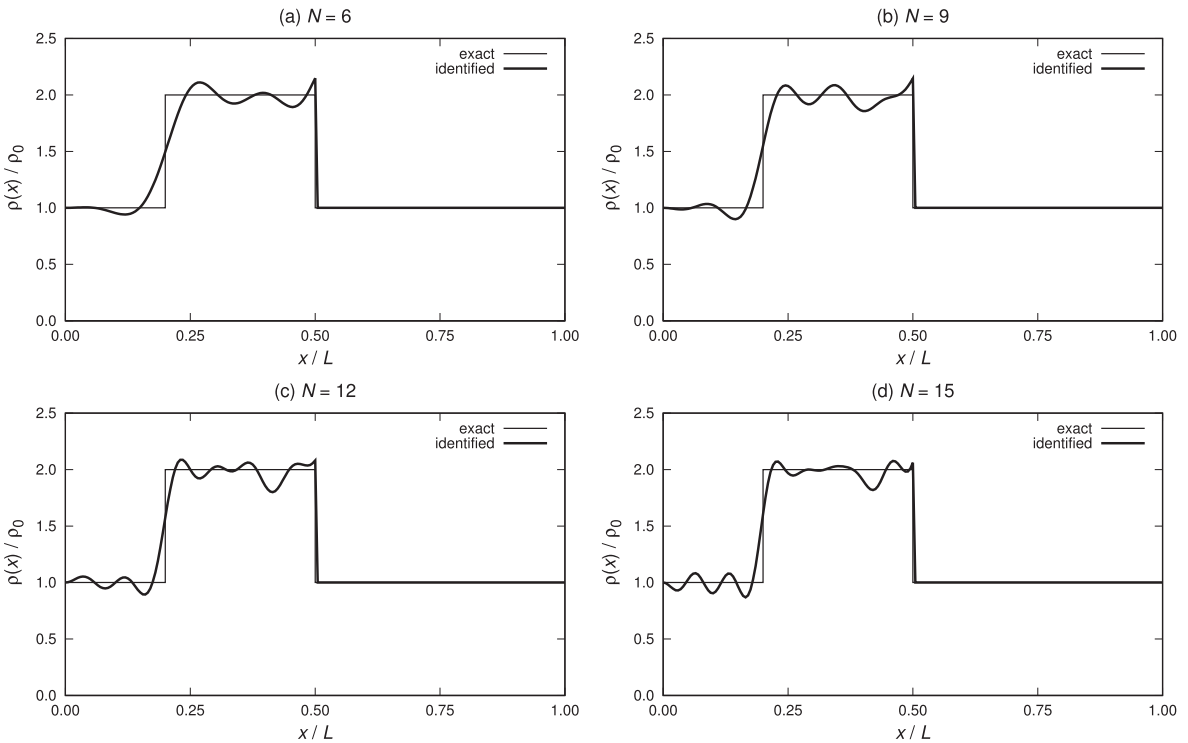

Fig. 7. Reconstruction of discontinuous mass changes as in (110), with $\frac{s}{L} = 0.35, \frac{\varepsilon}{L} = 0.30$, $t = 1.00$, using the first $N = 6, 9, 12, 15$ eigenfrequencies.

$$\rho(x) = \rho_0 + \rho_0 t \cdot \chi_{\left[s-\frac{c}{2}, s+\frac{c}{2}\right]}, \tag{110}$$

where s, c, t have the same meaning as in the previous section, see Fig. 1(b).

Since the mass density ρ has jump discontinuities at $x = s \pm \frac{c}{2}$, whereas the approximating functions $\Phi_n(x)$ are smooth functions of the axial coordinate x, it is expected that the reconstruction may fail near these points. Numerical simulations confirm this undesired behavior. Some representative cases are collected in Figs. 5 and 6.

These cases correspond to perturbations both located near the left end of the nanorod ($\frac{s}{L} = 0.15$) and with small support ($\frac{c}{L} = 0.1$), but having either small ($t = 0.1$, case i)) or large ($t = 1.0$, case ii)) intensity, respectively. In case i) (see Fig. 5), the results are accurate enough for $N = 15$, whereas the oscillations of the identified mass coefficient have appreciable amplitude in case ii) (see Fig. 6), and propagate in the remaining part of the interval $\left[0, \frac{L}{2}\right]$. The support of the perturbation is slightly overestimated and, as it was expected, L^∞ estimates fail near the jumps.

Fig. 7 collects the results for large mass variations, both in L^2 and in L^∞ norm, for $\frac{s}{L} = 0.35, \frac{c}{L} = 0.3, t = 1.0$. The support of the mass variation still is well estimated, even if oscillations with significant amplitude occur both within the support and in

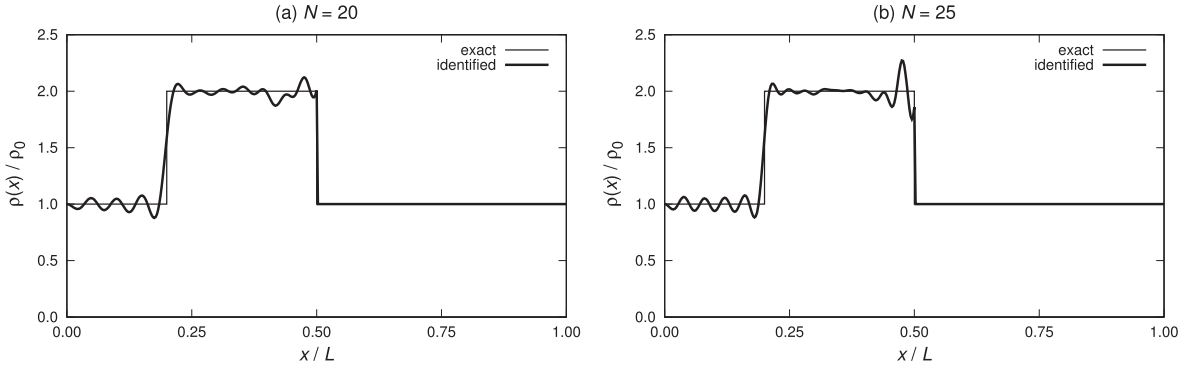

Fig. 8. Reconstruction of discontinuous mass changes as in (110), with $\frac{s}{L} = 0.35, \frac{c}{L} = 0.30$, $t = 1.00$, using the first $N = 20, 25$ eigenfrequencies.

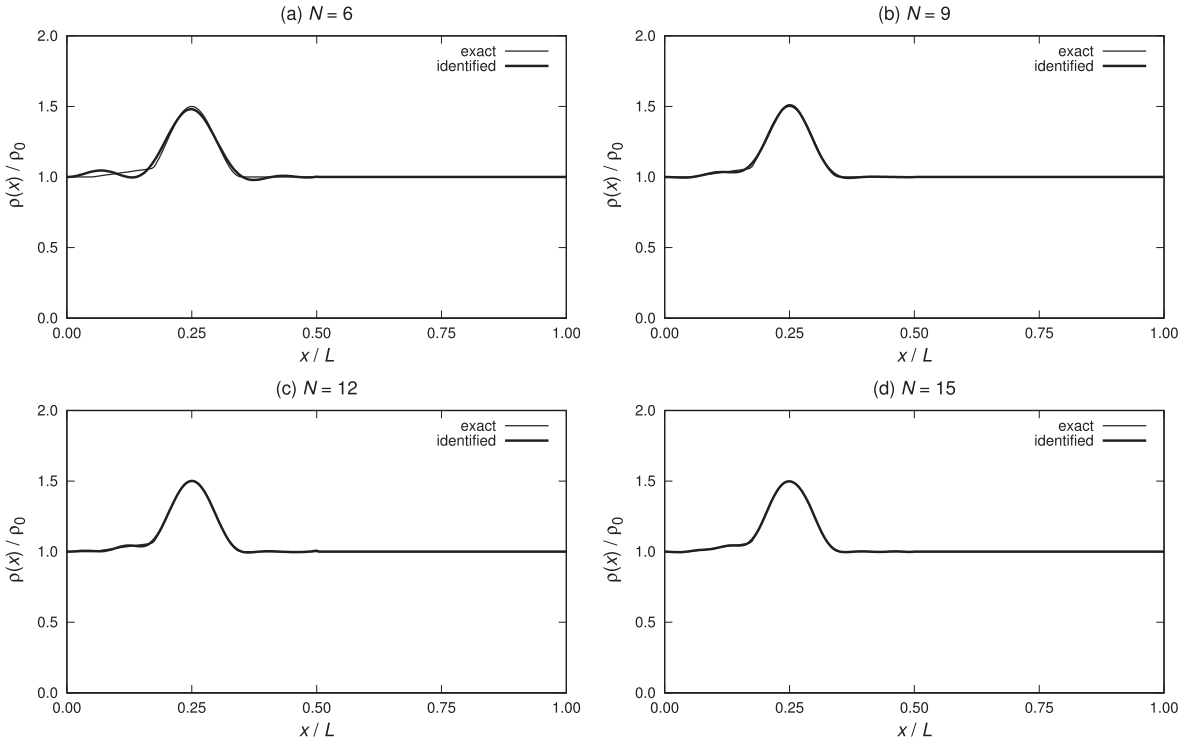

Fig. 9. Reconstruction of overlapping mass changes as in (111), with $\frac{s}{L} = 0.25, t = 0.50, \frac{s_1}{L} = 0.25, t_1 = 0.10$, using the first $N = 6$ to 15 eigenfrequencies.

the remaining part of the interval $\left[0, \frac{L}{2}\right]$. The number of iterations needed to satisfy the stopping criterion (63) is slightly bigger than the smooth case, being however always less than 10.

Finally, it can be shown that results generally improve by considering larger N, say $N = 20, 25$. In order to reduce the numerical approximation error on higher order eigenvalues, all these cases have been developed on a numerical model of the nanorod having $N_e = 400$ equally spaced finite elements. As it can be seen by comparing Figs. 7 and 8, the increase of N_e shows beneficial effects, such as more accurate estimate of the actual support of the mass variation and reduction of the amplitude of the spurious oscillations of the identified coefficient around the exact value. However, the identification of large mass variations with left (respectively, right) jump position close to the left end (respectively, to the mid point) of the nanorod still remains problematic to some extent.

5.3.3. Identification of overlapping added masses

The identification method has also been tested on mass distributions having less schematic profile than those considered in the previous sections. As an example, here we report some representative results related to two overlapping added mass profiles, one being regular (and belonging to the class of Section 5.3.1) and the other one having triangular shape, with a jump type discontinuity. More precisely, the mass density to be determined has the expression

$$\rho(x) = \rho_0 + \rho_0 \max\left\{ t\cos^2\left(\frac{\pi(x-s)}{c}\right)\chi_{\left[s-\frac{c}{2}, s+\frac{c}{2}\right]},\ \frac{t_1}{c_1}(x-(s_1-c_1))\chi_{[s_1-c_1, s_1]} \right\}, \tag{111}$$

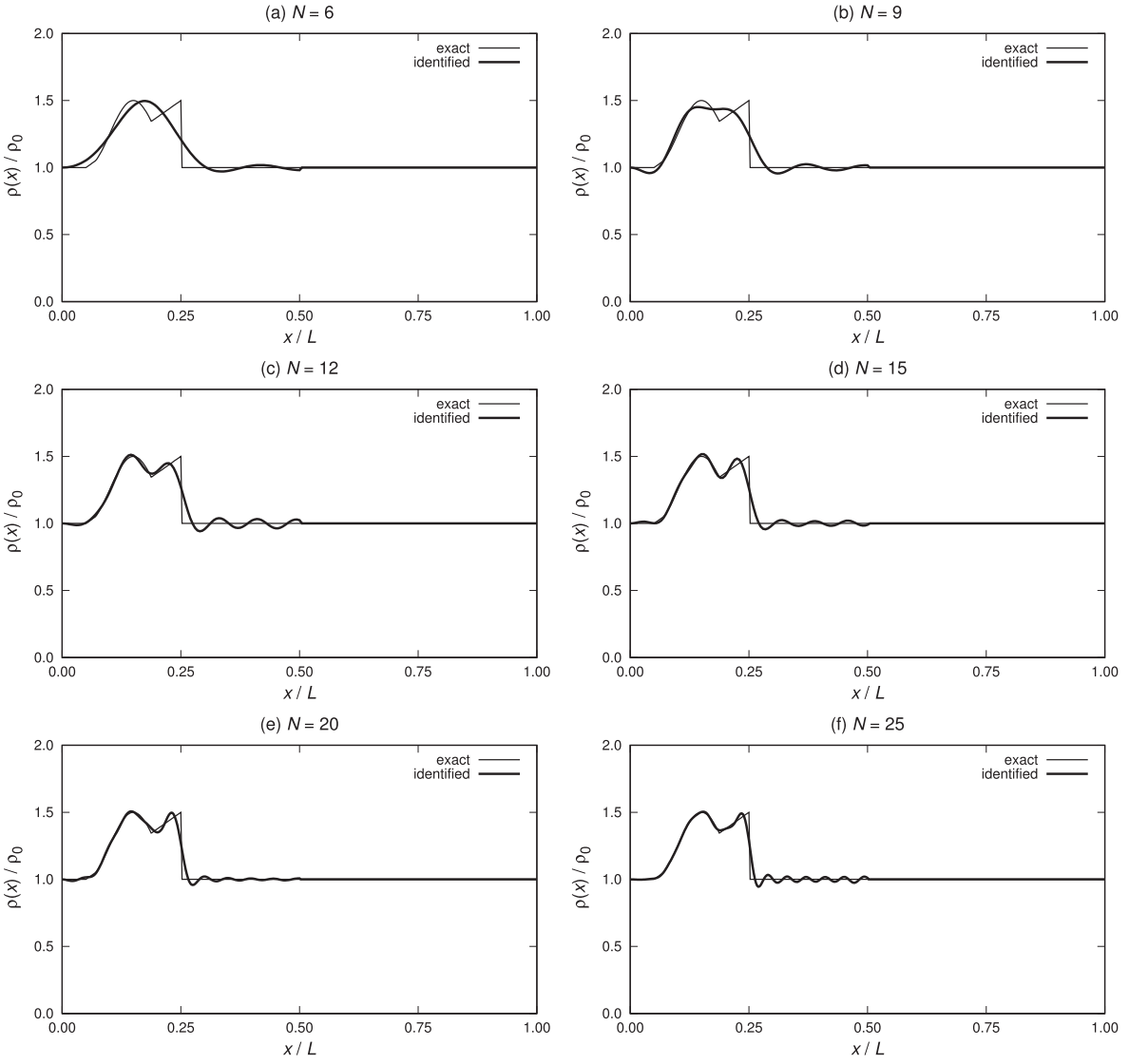

Fig. 10. Reconstruction of overlapping mass changes as in (111), with $\frac{s}{L} = 0.15, t = 0.50, \frac{s_1}{L} = 0.25, t_1 = 0.50$, using the first $N = 6$ to 25 eigenfrequencies.

where $[s_1 - c_1, s_1] \subset \left[0, \frac{L}{2}\right]$ and $t_1\rho_0, t_1 > 0$, is the support and the maximum value of the triangular added mass profile, respectively; see Fig. 1(c). Some of the results are summarized in the sequel. They have been obtained using $N_e = 200, 400$ equally spaced finite elements, for $N = 6, 9, 12, 15$ and $N = 20, 25$, respectively. In order to simplify the presentation of the results, the parameters c and c_1 have been assumed equal to $0.2L$. It should be noted that, depending on the values of s_1 and t_1, the coefficient $\rho(x)$ in (111) can be either continuous or discontinuous. The latter case occurs, for example, when $s_1 \in \left(s - \frac{c}{2}, s + \frac{c}{2}\right)$ and t_1 is small enough with respect to t.

The determination of continuous mass coefficient turns out to be very accurate even when only the first $9 - 12$ eigenfrequencies are used in identification, as it was found for the class of smooth variations considered in Section 5.3.1. We refer to Fig. 9 for a typical result.

In case of discontinuous coefficient, as it was already noticed in Section 5.3.2, spurious oscillations occur near the jump, with amplitude which turns out to be proportional to the intensity of the jump. As a consequence, identification of the smooth portion of the mass coefficient may become inaccurate for small values of t. At least $15 - 20$ first eigenfrequencies seem to be needed to obtain acceptable accuracy in these cases, see, for example, Fig. 10. The method also shows good ability in identifying mass variations with disjoint supports, particularly when the values of t_1 and t are close, see, for example, Fig. 11.

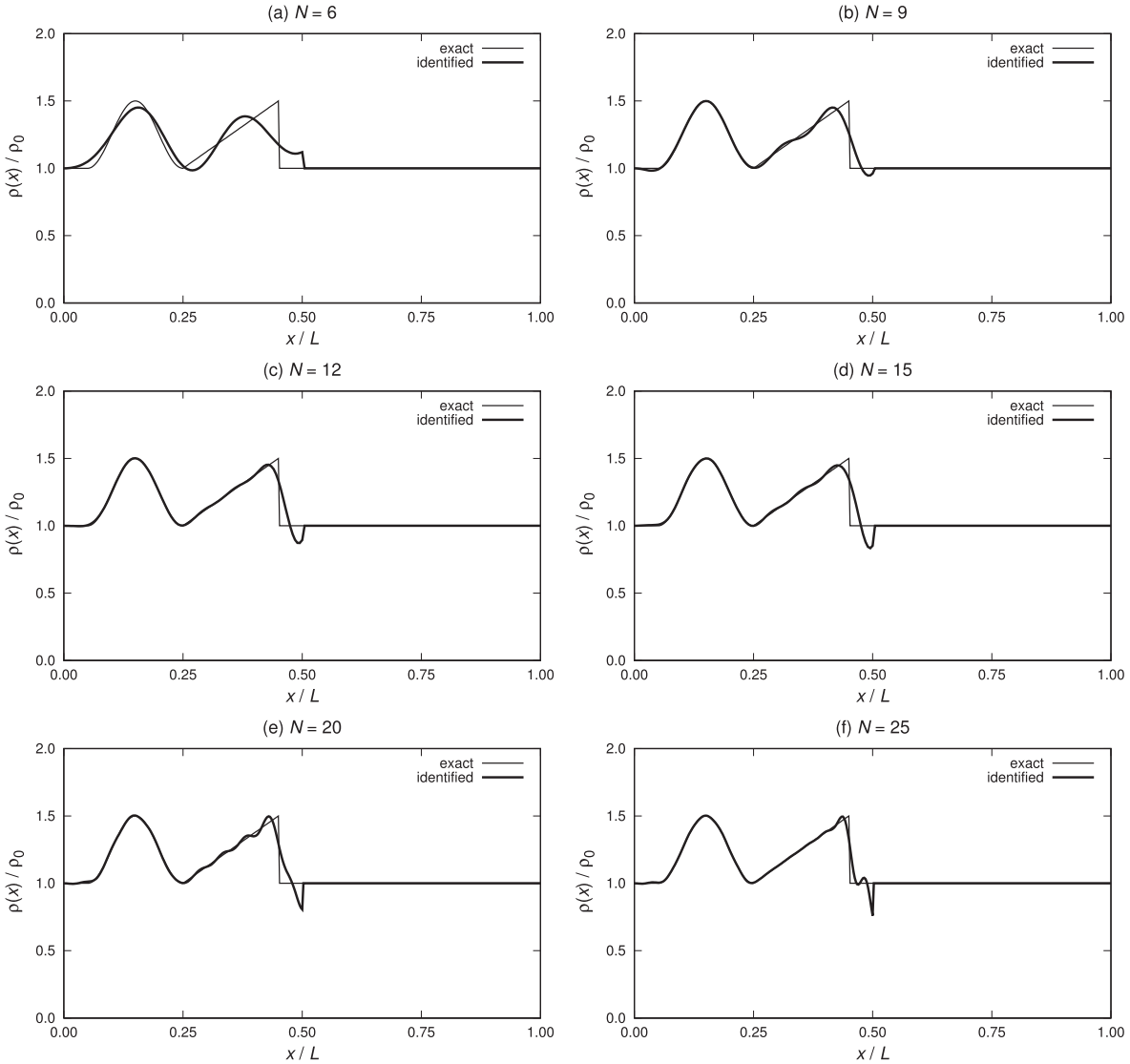

Fig. 11. Reconstruction of overlapping mass changes as in (111), with $\frac{s}{L} = 0.15, t = 0.50, \frac{s_1}{L} = 0.45, t_1 = 0.50$, using the first $N = 6$ to 25 eigenfrequencies.

5.3.4. Physical post-filtering

In this section we show that, when the method is combined with additional information about the unknown mass coefficient, such as monotonicity or a priori information on the support of the mass variation, the reconstruction may further improve, leading to good uniform approximation of the solution. More precisely, we have considered in the sequel the following a priori information:

F$_1$) The mass variation is positive, e.g., the condition (14) holds.
As remarked in Section 2, this information is simply available from the physics of the problem. Actually, our identification algorithm produces a function $\rho(x)$ which may oscillate near the unperturbed linear mass density ρ_0. Basing on assumption F_1, we *filter* the results of identification by setting the mass density to be ρ_0 whenever the reconstructed value of $\rho(x)$ is smaller than ρ_0.

F$_2$) There are situations in which it is a priori known that a *single* localized mass variation occurs in the nanosensor, that is, the support of the mass variation $r_\epsilon(x)$ is a closed (and possible small) interval compactly contained in $\left[0, \frac{L}{2}\right]$.
In this case, under the assumption that the reconstructed coefficient $\rho(x)$ is a good uniform approximation of the actual mass, one can determine the interval of maximum mass increase and neglect all the other possible regions on which the mass density increases.

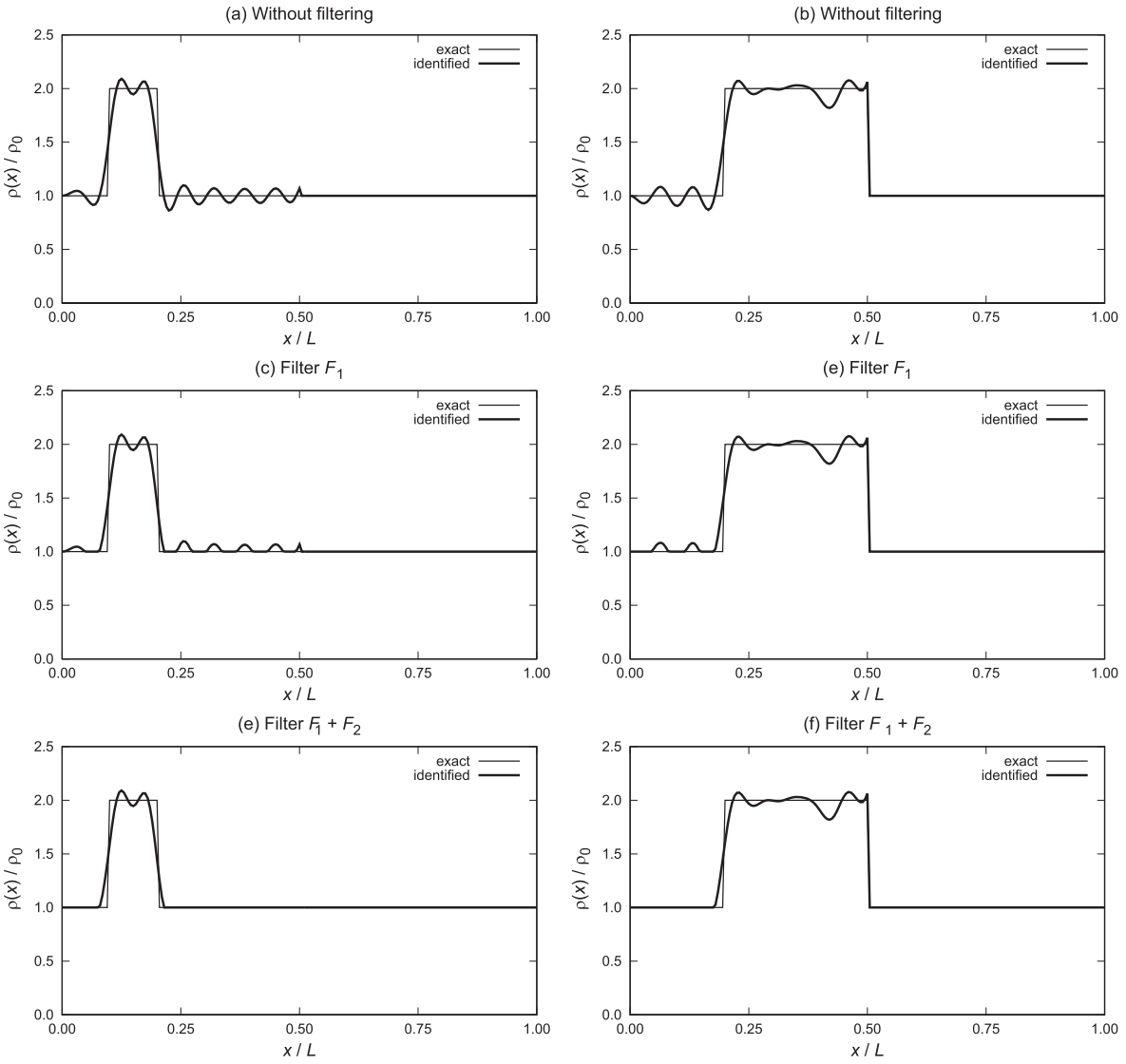

Fig. 12. Filtering effects on identification. Reconstruction of discontinuous mass changes as in (110), with $\frac{s}{L} = 0.15, \frac{c}{L} = 0.10$, $t = 1.00$, using the first $N = 15$ eigenfrequencies.

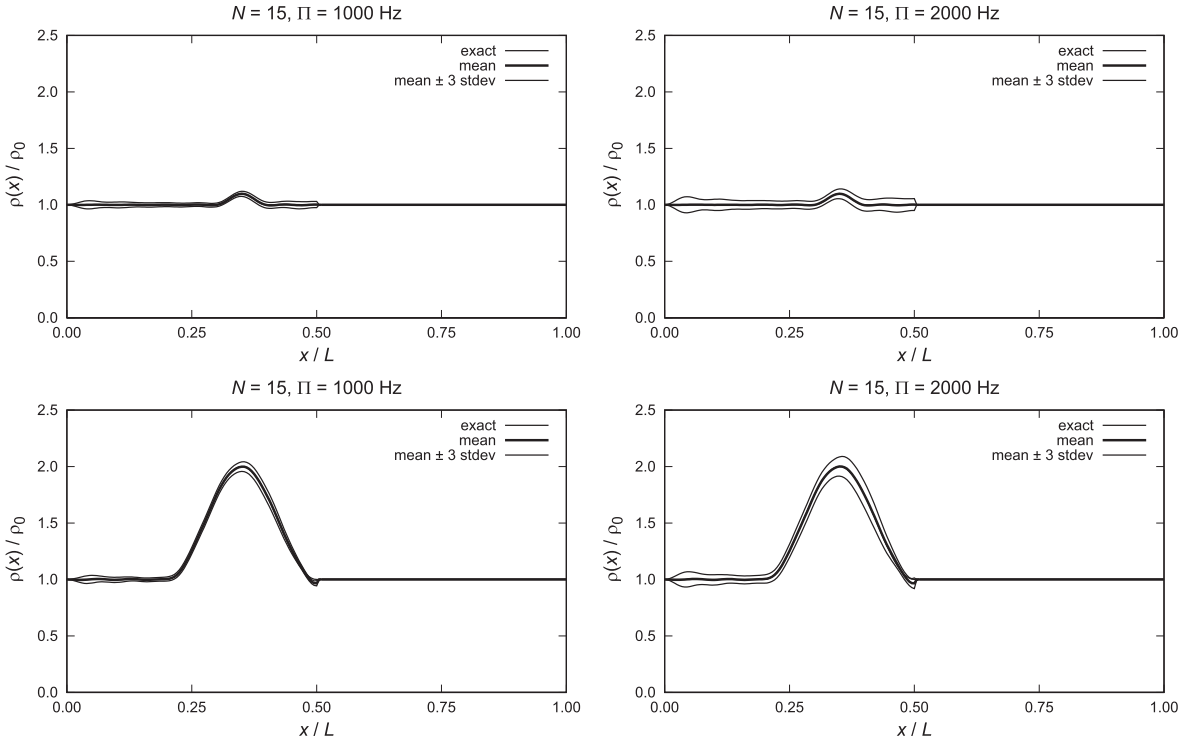

Fig. 13. Noise effects on identification of smooth mass changes. Upper row: mass changes as in (109), with $\frac{s}{L} = 0.35, \frac{c}{L} = 0.10$, $t = 0.10$. Lower row: mass changes as in (109), with $\frac{s}{L} = 0.35, \frac{c}{L} = 0.30$, $t = 1.00$.

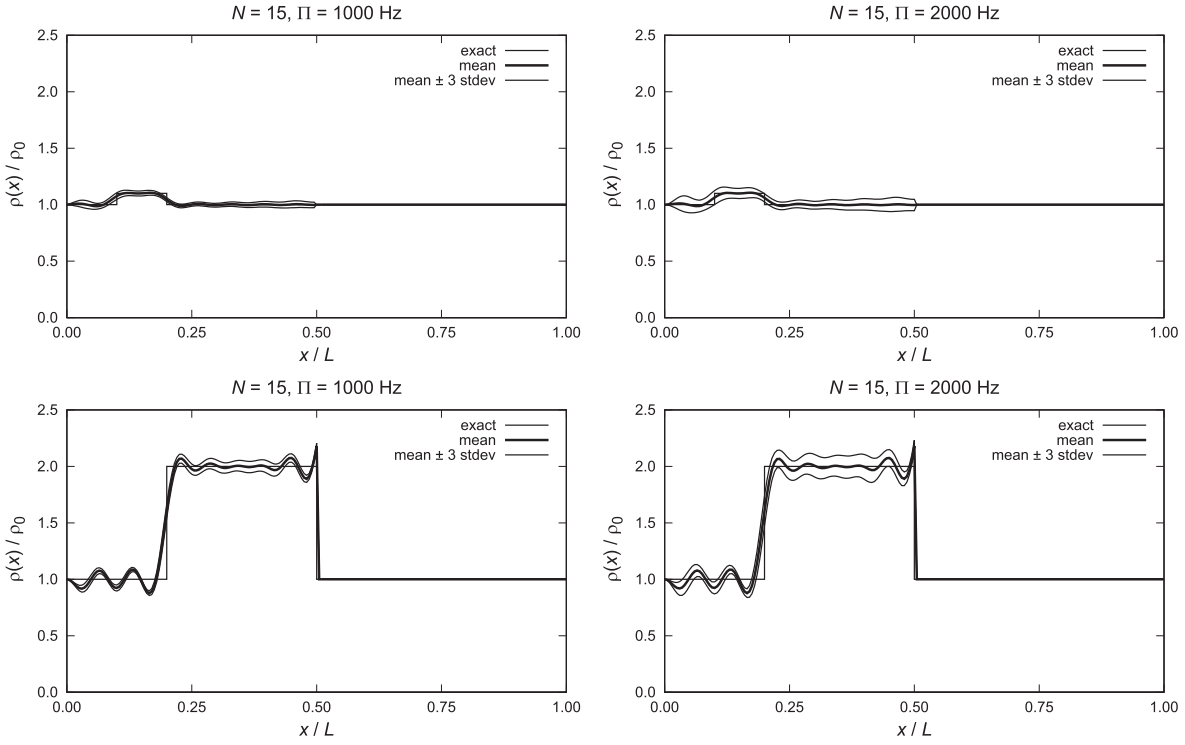

Fig. 14. Noise effects on identification of discontinuous mass changes. Upper row: mass changes as in (110), with $\frac{s}{L} = 0.15, \frac{c}{L} = 0.10$, $t = 0.10$. Lower row: mass changes as in (110), with $\frac{s}{L} = 0.35, \frac{c}{L} = 0.30$, $t = 1.00$.

In order to check how the identification results improve by adding the above hypotheses F_1 and F_2, we tested the method in an extended series of simulations with error free data. As an example, Fig. 12 reports the results obtained by applying filter F_1 and by combining in cascade $F_1 + F_2$. The cases considered correspond to discontinuous mass changes as in (110), with large mass variation ($t = 1.0$) localized either on a small or a large subinterval of $\left[0, \frac{L}{2}\right]$. The comparison with the corresponding unfiltered results clearly shows an improvement of accuracy of the reconstruction.

5.3.5. Application to noisy data

An important aspect for applications is stability against noise in the given spectral data. In order to test the robustness of the method, the identification was carried out by perturbing the target noise-free eigenvalue $\lambda_n^{exp}, n = 1, \ldots, N$ as follows

$$\sqrt{\lambda_n^{exp-err}} = \sqrt{\lambda_n^{exp}} + \tau_n. \tag{112}$$

Here, τ_n is a random Gaussian variable with vanishing mean and standard deviation $\hat{\sigma}$ such that $3\hat{\sigma} = 2\pi\Pi$, where Π is the maximum admitted error. The effect of errors was evaluated both for smooth and discontinuous mass distributions, by considering different profile of the coefficient and by varying the number N of the first eigenfrequencies used in identification, for increasing values of Π ranging from 100 Hz to 5000 Hz. A selected, though representative, set of results are presented in Figs. 13 and 14, for smooth and discontinuous mass coefficients, respectively. For each position along the nanorod axis, and besides the exact mass profile, every subfigure contains three curves: the curve of the mean value and the two curves obtained by adding $\pm 3\hat{\sigma}$ to the mean value. One thousand of simulations was performed for each case. It turns out that the three curves are almost indistinguishable for $\Pi = 100$ Hz. Appreciable discrepancy occurs for $\Pi = 1000$ Hz, and for Π greater than 3000 Hz the accuracy of the reconstruction is seriously compromised. In particular, for Π less than 2000 Hz, the effect of errors makes it possible to discriminate the presence of even minor variations of mass, either regular or discontinuous, and for which the influence of errors on data is expected to be more significant. It should be noted that $\Pi = 2000$ Hz corresponds to percentage errors ranging from 0.05 (high frequency) to 0.65 (low frequency) per cent of the unperturbed first fifteen resonant frequencies. Finally, the convergence speed of the iterative method is not significantly affected by the random noise, and the number of iterations needed to get convergence is slightly bigger than in the error-free case. The condition number $\kappa(\mathbf{A})$ takes values of the same order of those found in the analysis of the corresponding cases in absence of errors on the data.

6. Conclusions

The mass sensing principle for nanoresonators sensors is based on monitoring the variations of the resonant frequencies caused by unknown additional masses attached on the surface of a referential system. In spite of important applications in physical, chemical and biological fields, to the authors knowledge, a general formulation of the inverse problem of identifying distributed added mass attached on nanostructures, within the framework of generalized continuum mechanics theories, it has not been developed until now. The present work is a first contribution on this topic.

We have investigated the inverse problem of determining additional distributed mass on a nanorod from finite number of natural frequencies of the free axial vibration and partial knowledge of the unknown mass coefficient. Under the assumption that the nanorod is clamped at the ends and the mass is given on half of the nanosensor, a reconstruction method has been proposed. The method consists of a sequence of linearizations of the inverse problem, and results in the construction of an approximating mass density that has the given (measured) first N eigenvalues.

When the method is applied near the unperturbed uniform nanorod, the reconstructed mass coefficient resembles a generalized Fourier partial sum of order N expressed on a suitable class of functions, each of which is the gradient of the nth eigenvalue with respect to the mass variation. Therefore, the quantity of data required by the method to obtain good approximation of the mass coefficient depends on the smoothness of the coefficient. The results of an extensive series of simulations indicate that for smooth (e.g., at least continuous) coefficients the high order Fourier contributions are less important and few eigenvalues, N less then 10, provide sufficient data for a good uniform approximation. When the mass variation is rough (e.g., discontinuous), then some of the higher order Fourier coefficients are significant and eigenvalues corresponding to the higher modes will needed to capture the actual behavior, i.e., $N = 15 - 20$. In general, the smoother the coefficient, the more rapidly the method converges with small error in L^∞-norm. Often, the first few iterates exhibit a good deal of oscillation. The rougher the coefficient, the more pronounced was this behavior and the amplitude of the oscillations around the exact coefficient. This seems in agreement with the behavior observed in previous studies on second order Sturm-Liouville operators, see, among other contributions, [37,45–47].

We have also provided a convergence theorem to the solution of the inverse problem for a particular family of finite dimensional coefficients. The result holds under the assumption that the eigenvalues of the unperturbed and perturbed nanorod are close enough, and the mass variation is sufficiently small in norm. Presumably, the basic idea of the proof can be extended also to some other cases, such as those in which two spectra are used to reconstruct a general mass variation on the whole interval axis, but is seems unlikely that the two above mentioned assumptions can be removed.

In spite of the mathematical difficulties typical for this class of finite inverse eigenvalue problems, numerical simulations show accurate approximation using L^2 or even L^∞ norms, which, in principle, is possible when using an infinite amount of data only. In particular, our experience shows that the accuracy of the method increases when spectral data are used in conjunction with additional information about the unknown coefficient, such as the positivity of the function expressing the increase of mass, which is available simply from the physics of the problem. Finally, it is interesting to notice that the method shows unexpected ability to reconstruct not necessarily small (smooth) mass variations, without the need of introducing further information on the unknown coefficient, such as the average of the unknown coefficient that, generally, needs knowledge of asymptotic expression of eigenvalues. It would be interesting to investigate on general properties on this issue.

Acknowledgements

The authors from Universidad Carlos III de Madrid wish to acknowledge Ministerio de Economía y Competitividad de España for the financial support, under Grant No. DPI2014-57989-P. The authors from University of Udine gratefully acknowledge the financial support of the National Research Project PRIN 2015TT JN95 'Identification and monitoring of complex structural systems'.

Appendix A

In this Appendix we prove Theorem 3.1.

Let n be a fixed integer, $n \geqslant 1$.

Proof of estimate (33).

We adapt the arguments shown in [33]. The Rayleigh quotient for the eigenvalue problem (15)–(17) is

$$R[u,\rho] = \frac{\int_0^L b(u'')^2 + a(u')^2}{\int_0^L \rho u^2}, \tag{113}$$

for every function $u \in \mathcal{H} \setminus \{0\}$, that is, $u \in H^2(0,L)$ satisfying the end conditions $u(0) = u(L) = 0$.

Let us recall the following variational characterization of the eigenvalues of (15)–(17). Let $v_n(x;\rho)$ denote the eigenfunction corresponding to $\lambda_n(\rho)$ and let $\mathcal{U}_n(\rho)$ be the subspace of $\mathcal{H}$ spanned by the first n eigenfunctions $\{v_1(x;\rho),\dots,v_n(x;\rho)\}$. Let V_n be any other n-dimensional subspace of $\mathcal{H}$. We have

$$\lambda_n(\rho) \leqslant \max_{u \in V_n \setminus \{0\}} R[u,\rho], \qquad \lambda_n(\rho) = \max_{u \in \mathcal{U}_n(\rho) \setminus \{0\}} R[u,\rho]. \tag{114}$$

For every function $u \in \mathcal{H} \setminus \{0\}$ we have

$$R[u,\rho_2] = R[u,\rho_1]\left(1 + \frac{\int_0^L (\Delta\rho)u^2}{\int_0^L \rho_2 u^2}\right), \tag{115}$$

with $\Delta\rho = \rho_1 - \rho_2$.

Our main goal is to show that the numerator of the fraction appearing on the right hand side of (115) can be bounded from above by $const.\|\Delta\rho\|_2 \int_0^L u^2$ for every $u \in \mathcal{U}_n(\rho_1) \setminus \{0\}$, where *const.* is a positive constant depending only on the a priori data and n. In fact, on assuming this bound available, and using the uniform lower bound (13), from (115) we have

$$R[u,\rho_2] \leqslant R[u,\rho_1](1 + C\|\Delta\rho\|_2), \tag{116}$$

where the constant $C > 0$ only depends on the a priori data and n. Next, taking the maximum in (116) over the functions $u \in \mathcal{U}_n(\rho_1) \setminus \{0\}$ and using the variational characterization (114), we obtain

$$\lambda_n(\rho_2) \leqslant \lambda_n(\rho_1)(1 + C\|\Delta\rho\|_2). \tag{117}$$

Reversing the indexes 1 and 2, we also have

$$\lambda_n(\rho_1) \leqslant \lambda_n(\rho_2)(1 + C\|\Delta\rho\|_2). \tag{118}$$

From (117) and (118) we can derive the inequality

$$|\lambda_n(\rho_2) - \lambda_n(\rho_1)| \leqslant C \max\{\lambda_n(\rho_1), \lambda_n(\rho_2)\}\|\Delta\rho\|_2. \tag{119}$$

Recalling that, by definition of ρ^- in (13) and by monotonicity results (see, for example, [41]), we have $\lambda_n(\rho_1) \leqslant \lambda_n(\rho^-)$ and $\lambda_n(\rho_2) \leqslant \lambda_n(\rho^-)$ for every $n \geqslant 1$, the wished estimate (33) follows from (120).

To complete the proof, it remains to control the numerator in the fraction on the right hand side of (115).

Let $u \in \mathcal{U}_n(\rho_1) \setminus \{0\}$, that is $u(x) = \sum_{i=1}^n c_i v_i(x;\rho_1)$ with $\sum_{i=1}^n c_i^2 > 0$, where $v_i(x;\rho_1)$ is normalized so that $\int_0^L \rho_1 v_1^2(x;\rho_1) = 1, i = 1,\dots,n$. By integrating by parts, we have:

$$\int_0^L \Delta\rho(x)u^2(x)dx = u^2(x)\int_0^x \Delta\rho(x_1)dx_1|_{x=0}^{x=L} - \int_0^L \left(\int_0^x \Delta\rho(x_1)dx_1\right)(u^2(x))'dx$$
$$= -2\int_0^L \left(\int_0^x \Delta\rho(x_1)dx_1\right)u(x)u'(x)dx. \tag{120}$$

Using Hölder inequality, we obtain $|\int_0^x \Delta\rho(x_1)dx_1| \leqslant L^{\frac{1}{2}}\|\Delta\rho\|_2$, and then, inserting this estimate in (120), we get

$$|\int_0^L \Delta\rho(x)u^2(x)dx| \leqslant 2L^{\frac{1}{2}}\|\Delta\rho\|_2 \int_0^L |u(x)u'(x)|dx \leqslant 2L^{\frac{1}{2}}\|\Delta\rho\|_2\ \|u\|_2\ \|u'\|_2. \tag{121}$$

In order to estimate $\|v_i'\|_2$, by the weak formulation of the eigenvalue problem for $\{\lambda_i(\rho_1), v_i(x;\rho_1)\}$, and recalling that $\int_0^L \rho_1 v_i^2(x;\rho_1) = 1$, we have

$$\int_0^L \left(v_i'(x;\rho_1)\right)^2 \leqslant \frac{\lambda_i(\rho_1)}{a}, \tag{122}$$

for every $i \geqslant 1$. Then, by Schwarz inequality and (122), we have

$$\int_0^L (u'(x))^2 \leqslant \sum_{i=1}^n c_i^2 \cdot \sum_{i=1}^n \int_0^L \left(v_i'(x;\rho_1)\right)^2 \leqslant \frac{1}{a}\cdot\sum_{i=1}^n \lambda_i(\rho_1)\cdot\sum_{i=1}^n c_i^2. \tag{123}$$

By the orthogonality of the eigenfunctions $v_i(x;\rho_1)$ we also have

$$\int_0^L \rho_1 u^2(x) = \int_0^L \rho_1\left(\sum_{i=1}^n c_i v_i(x;\rho_1)\right)^2 = \sum_{i=1}^n c_i^2, \tag{124}$$

and (123) becomes

$$\int_0^L (u'(x))^2 \leqslant \frac{\rho^+}{a}\cdot\sum_{i=1}^n \lambda_i(\rho_1)\int_0^L u^2(x). \tag{125}$$

Finally, using (125) in (121), we obtain

$$\left|\int_0^L \Delta\rho(x)u^2(x)dx\right| \leqslant 2L^{\frac{1}{2}}\|\Delta\rho\|_2\left(\frac{\rho^+}{a}\cdot\sum_{i=1}^n \lambda_i(\rho_1)\right)^{\frac{1}{2}}\|u\|_2^2. \tag{126}$$

By monotonicity results, we have $\lambda_i(\rho_1) \leqslant \lambda_i(\rho^-) \leqslant \lambda_n(\rho^-)$, for every $i = 1,\dots,n$. It follows that estimate (116) can be obtained from inequality (115), and the proof is complete.

Proof of estimate (35).

We now consider the continuity of the nth eigenfunction with respect to the mass coefficient.

Let us represent the nth eigenfunction $v_n(x;\rho_2)$ on the Hilbertian basis of $\mathcal{H}$ formed by the eigenfunctions $\{v_k(x;\rho_1)\}_{k=1}^\infty$:

$$v_n(x;\rho_2) = \sum_{k=1}^\infty c_n^k v_k(x;\rho_1), \tag{127}$$

where the series is uniformly convergent in $\mathcal{H}$ up to the second order derivatives.

Coefficients $\{c_n^k\}_{k=1}^\infty$ depend on ρ_1,ρ_2, e.g., $c_n^k = c_n^k(\rho_1,\rho_2)$. In view of the condition $v_n'(0;\rho_1)v_n'(0;\rho_2) > 0$ assumed in Theorem 3.1, we require that, for $i = 1,2$, $c_n^n(\rho_i,\rho_i) = 1$ and $c_n^k(\rho_i,\rho_i) = 0$ if $k \neq n$.

Let us notice that, by (127), we have

$$v_n(x;\rho_2) - v_n(x;\rho_1) = \sum_{k=1,k\neq n}^\infty c_n^k v_k(x;\rho_1) + (c_n^n - 1)\,v_n(x;\rho_1). \tag{128}$$

Therefore, in order to estimate $\|v_n(x;\rho_2) - v_n(x;\rho_1)\|_2$, we need to control the sequence $\{c_n^k\}_{k=1,k\neq n}^\infty$ and the term $|c_n^n - 1|$.

Let us recall the weak formulation of the eigenvalue problem (15)–(17) for $\{\lambda_n(\rho_2), v_n(x;\rho_2)\}$:

$$\int_0^L \left(bv_n''(x;\rho_2)\varphi'' + av_n'(x;\rho_2)\varphi'\right) = \lambda_n(\rho_2)\int_0^L \rho_2 v_n(x;\rho_2)\varphi, \tag{129}$$

for every $\varphi \in \mathcal{H}$. By inserting (127) in (129), choosing $\varphi = v_j(x;\rho_1), j \geqslant 1$, and using the orthogonality conditions

$$\int_0^L \rho_1 v_k(x;\rho_1)v_j(x;\rho_1) = \delta_{kj}, \quad k,j \geqslant 1, \tag{130}$$

we have

$$c_n^j(\lambda_n(\rho_2)-\lambda_j(\rho_1)) = -\lambda_n(\rho_2)\int_0^L(\rho_2-\rho_1)v_n(x;\rho_2)v_j(x;\rho_1), \tag{131}$$

for every $j \geqslant 1$.

In order to simplify the notation, in the sequel we shall denote by C a positive constant that depends on the a priori data only and n, and that may change from line to line.

It should be noted that if $j = n$ in (131), then the left and the right hand side can be made very small for $\rho_1 \approx \rho_2$, and in the limit $\rho_2 = \rho_1$ Eq. (131) degenerates into a trivial identity. Therefore, we first assume $j \neq n$ and we estimate from below the quantity $(\lambda_n(\rho_2)-\lambda_j(\rho_1))$. The case $j = n$ shall be discussed later on.

We notice that, by asymptotic eigenvalue estimates, there exists $J_0^* \in \mathbb{N}$ and there exists a positive constant C such that

$$\frac{C}{2}j^4 \leqslant \lambda_j(\rho_1) \leqslant Cj^4, \qquad \text{for } j > J_0^*. \tag{132}$$

Let us distinguish two cases.

First, let $j > J_0^*$. By (132), one can show that there exists a number $J_0 \in \mathbb{N}, J_0$ possibly bigger than J_0^* and $J_0 > n$, such that

$$|\lambda_n(\rho_2)-\lambda_j(\rho_1)| \geqslant Cj^4, \qquad \text{for } j > J_0, \tag{133}$$

and, therefore,

$$\left|\frac{\lambda_n(\rho_2)}{\lambda_n(\rho_2)-\lambda_j(\rho_1)}\right| \leqslant \frac{C}{j^4}, \qquad \text{for } j > J_0. \tag{134}$$

In the other case, e.g., $j \leqslant J_0$ and $j \neq n$, we notice that there exists $\widehat{\epsilon}, \widehat{\epsilon}$, $0 < \widehat{\epsilon} < 1$ only depending on the a priori data and n, such that the sequences $\{\lambda_n(\rho_1)\}_{n=1}^{\infty}$, $\{\lambda_n(\rho_2)\}_{n=1}^{\infty}$ are uniformly discrete with separation constant $\sigma/2$, provided that $\|\rho_i - \rho_0\|_2 \leqslant \epsilon$ for $0 < \epsilon \leqslant \widehat{\epsilon}, i = 1, 2$. This property follows from the fact that the sequence $\{\lambda_n\}_{n=1}^{\infty}$ is uniformly discrete (with separation constant σ) and by using the continuity of the eigenvalues with respect to small L^2-perturbations of the referential linear mass density ρ_0 (e.g., for $\widehat{\epsilon}$ small enough).

Therefore, we can estimate from below as follows:

$$|\lambda_n(\rho_2)-\lambda_j(\rho_1)| \geqslant \min\{|\lambda_n(\rho_2)-\lambda_{n-1}(\rho_1)|, |\lambda_n(\rho_2)-\lambda_{n+1}(\rho_1)|\}, \tag{135}$$

where we have assumed $\lambda_0(\rho_1) = 0$. Let us consider the first term on the right hand side, the analysis of the second being similar. Since the sequence $\{\lambda_n(\rho_2)\}_{n=1}^{\infty}$ is uniformly discrete with separation constant $\sigma/2$, using estimate (33), and reducing the value of $\widehat{\epsilon}$ (where $\widehat{\epsilon}$ only depends on the a priori data and n), we have

$$|\lambda_n(\rho_2)-\lambda_{n-1}(\rho_1)| \geqslant |\lambda_n(\rho_2)-\lambda_{n-1}(\rho_2)| - |\lambda_{n-1}(\rho_2)-\lambda_{n-1}(\rho_1)| \geqslant \frac{\sigma}{2} - C_{n-1}^{\lambda}\|\rho_2-\rho_1\|_2 \geqslant \frac{\sigma}{4}. \tag{136}$$

Therefore, for every $j \leqslant J_0$ and $j \neq n$, we have

$$\left|\frac{\lambda_n(\rho_2)}{\lambda_n(\rho_2)-\lambda_j(\rho_1)}\right| \leqslant C. \tag{137}$$

By (134) and (137), we can compute c_n^j for $j \neq n$:

$$c_n^j = -\frac{\lambda_n(\rho_2)}{\lambda_n(\rho_2)-\lambda_j(\rho_1)}\int_0^L(\rho_2-\rho_1)v_n(x;\rho_2)v_j(x;\rho_1). \tag{138}$$

By adapting the arguments used to prove (37), $v_n(x;\rho_2)$ is uniformly bounded in $[0, L]$, i.e.,

$$\max_{x\in[0,L]}|v_n(x;\rho_2)| \leqslant C. \tag{139}$$

Then, by applying Hölder inequality to (138) and using (139), we have

$$|c_n^j| \leqslant C\left|\frac{\lambda_n(\rho_2)}{\lambda_n(\rho_2)-\lambda_j(\rho_1)}\right| \|\rho_2-\rho_1\|_2, \tag{140}$$

that is, by (134) and (137),

$$|c_n^j| \leqslant C\|\rho_2-\rho_1\|_2, \quad j \leqslant J_0,\ j \neq n, \tag{141}$$

$$|c_n^j| \leqslant \frac{C}{j^4}\|\rho_2-\rho_1\|_2, \quad j > J_0. \tag{142}$$

We are now in position to estimate the L^2 norm (squared) of the first term appearing on the right hand side of (128):

$$\int_0^L \left(\sum_{k=1,k\neq n}^{\infty} c_n^k v_k(x;\rho_1)\right)^2 \leqslant \int_0^L \left(\sum_{k=1,k\neq n}^{J_0} c_n^k v_k(x;\rho_1)\right)^2 + 2\int_0^L \left(\sum_{k=J_0+1}^{\infty} c_n^k v_k(x;\rho_1)\right)^2 \equiv 2\left(I_{J_0}+I_\infty\right). \tag{143}$$

Let us first consider I_{J_0}. By Schwarz's inequality and (141), we have

$$I_{J_0} \leqslant \int_0^L \left(\sum_{k=1,k\neq n}^{J_0} \left(c_n^k\right)^2\right)\cdot\left(\sum_{k=1,k\neq n}^{J_0} \left(v_k(x;\rho_1)\right)^2\right) \leqslant C\|\rho_2-\rho_1\|_2^2. \tag{144}$$

Concerning the term I_∞, we use the asymptotic estimate (142) and Schwarz inequality, obtaining

$$\begin{aligned} I_\infty &\leqslant \int_0^L \left(\sum_{k=J_0+1}^{\infty} c_n^k v_k(x;\rho_1)\right)^2 \leqslant \int_0^L \left(\sum_{k=J_0+1}^{\infty} k^2\left(c_n^k\right)^2\right)\cdot\left(\sum_{k=J_0+1}^{\infty}\frac{1}{k^2}\left(v_k(x;\rho_1)\right)^2\right) \\ &\leqslant \sum_{k=J_0+1}^{\infty} k^2\frac{C^2\|\rho_2-\rho_1\|_2^2}{k^8}\cdot\sum_{k=J_0+1}^{\infty}\frac{1}{k^2}\int_0^L \left(v_k(x;\rho_1)\right)^2 \leqslant C\|\rho_2-\rho_1\|_2^2\sum_{k=1}^{\infty}\frac{1}{k^6}\cdot\sum_{k=1}^{\infty}\frac{1}{k^2} \leqslant C\|\rho_2-\rho_1\|_2^2. \end{aligned} \tag{145}$$

Inserting (144) and (145) in (143), we obtain

$$\|\sum_{k=1,k\neq n}^{\infty} c_n^k v_k(x;\rho_1)\|_2 \leqslant C\|\rho_2-\rho_1\|_2. \tag{146}$$

Finally, let us evaluate c_n^n. Recalling the normalization conditions (34), and using the representation (127), we have

$$\begin{aligned} &\left(c_n^n\right)^2\int_0^L \rho_1 v_n^2(x;\rho_1) + \sum_{j=1,j\neq n}^{\infty} c_n^n c_n^j\int_0^L \rho_1 v_n(x;\rho_1)v_j(x;\rho_1) + \sum_{k=1,k\neq n}^{\infty} c_n^n c_n^k\int_0^L \rho_1 v_n(x;\rho_1)v_k(x;\rho_1) \\ &+ \sum_{k,j=1,\ (k,j)\neq(n,n)}^{\infty} c_n^k c_n^j\int_0^L \rho_1 v_k(x;\rho_1)v_j(x;\rho_1) = \int_0^L \rho_1 v_n^2(x;\rho_1). \end{aligned} \tag{147}$$

By the orthogonality conditions (130), the above equation reduces to

$$\left(c_n^n\right)^2 - 1 = -\sum_{j=1,j\neq n}^{\infty}\left(c_n^j\right)^2, \tag{148}$$

where the right hand side can be estimated, as before, by using (141) and (142), that is

$$\left(c_n^n\right)^2 \leqslant 1 + C\|\rho_2-\rho_1\|_2^2. \tag{149}$$

By choosing $\widehat{\epsilon}>0$ small enough, and recalling that c_n^n is expected to belong to a neighborhood of 1 (e.g., $c_n^n(\rho_i,\rho_i)=1, i=1,2$), the above equality implies

$$|c_n^n - 1| \leqslant C\|\rho_2-\rho_1\|_2^2, \tag{150}$$

that is the second term in (128) is an higher order term with respect to $\|\rho_2-\rho_1\|_2$, and the thesis (35) follows.

Remark 6.1. We conclude this Appendix by proving that, under the assumptions of Theorem 3.1, the eigenfunctions are continuous in the H^2 norm with respect to mass perturbation. To show this, let us start with the following identity, which involves the energy norm $|||\cdot|||$ of the difference $(v_n(x;\rho_1)-v_n(x;\rho_2))$:

$$\begin{aligned} |||v_n(x;\rho_2)-v_n(x;\rho_1)|||^2 &\equiv \int_0^L b\left(v_n''(x;\rho_2)-v_n''(x;\rho_1)\right)^2 + a\left(v_n'(x;\rho_2)-v_n'(x;\rho_1)\right)^2 \\ &= \int_0^L b\left(v_n''(x;\rho_1)\right)^2 + a\left(v_n'(x;\rho_1)\right)^2 - \int_0^L \left(b v_n''(x;\rho_1)v_n''(x;\rho_2) + a v_n'(x;\rho_1)v_n'(x;\rho_2)\right) \\ &\quad + \int_0^L \left(b v_n''(x;\rho_2)\left(v_n''(x;\rho_2)-v_n''(x;\rho_1)\right) + a v_n'(x;\rho_2)\left(v_n'(x;\rho_2)-v_n'(x;\rho_1)\right)\right) \\ &\equiv I_1+I_2+I_3, \end{aligned} \tag{151}$$

for every $n\geqslant 1$. By the weak formulation of the eigenvalue problem (see, for example, (129)), we have

$$I_1 = \lambda_n(\rho_1)\int_0^L \rho_1 v_n^2(x;\rho_1), \tag{152}$$

$$I_2 = -\lambda_n(\rho_1)\int_0^L \rho_1 v_n(x;\rho_1)v_n(x;\rho_2), \tag{153}$$

$$I_3 = \lambda_n(\rho_2)\int_0^L \rho_2 v_n(x;\rho_2)(v_n(x;\rho_2) - v_n(x;\rho_1)), \tag{154}$$

where the functions $v_n(x;\rho_2)$ and $(v_n(x;\rho_2) - v_n(x;\rho_1))$ have been chosen as test functions to obtain (153) and (154), respectively. Therefore, by inserting (152)–(154) in (151), we have

$$|||v_n(x;\rho_2) - v_n(x;\rho_1)|||^2 = \lambda_n(\rho_1)\int_0^L \rho_1 v_n(x;\rho_1)(v_n(x;\rho_1) - v_n(x;\rho_2)) + \lambda_n(\rho_2)\int_0^L \rho_2 v_n(x;\rho_2)(v_n(x;\rho_2) - v_n(x;\rho_1)). \tag{155}$$

By using Hölder inequality, the normalization conditions (34) and estimate (35), we have

$$|||v_n(x;\rho_2) - v_n(x;\rho_1)|||^2 \leqslant C\|v_n(x;\rho_2) - v_n(x;\rho_1)\|_2 \leqslant C\|\rho_1 - \rho_2\|_2, \tag{156}$$

where $C > 0$ is a constant only depending on the a priori data and n. It should be noted that, if $\rho_1 = \rho_0$ (unperturbed nanorod) and $\rho_2 = \rho_0 + r_\epsilon(x)$ (see (11)), for $\epsilon > 0$ small enough, then the energy norm $|||v_n(x;\rho_0) - v_n(x;\rho_0 + r_\epsilon(x))|||$ is of order $\epsilon^{1/2}$ instead of order ϵ, as for the norm $\|v_n(x;\rho_0) - v_n(x;\rho_0 + r_\epsilon(x))\|_2$. Finally, using (35) and (156), one can obtain the wished H^2 estimate:

$$\|v_n(x;\rho_2) - v_n(x;\rho_1)\|^2_{H^2(0,L)} \leqslant C\|\rho_1 - \rho_2\|_2, \tag{157}$$

where the constant $C > 0$ only depends on the a priori data and n.

References

[1] X. Li, H. Yu, X. Gan, X. Xia, P. Xu, J. Li, M. Liu, Y. Li, Integrated MEMS/NEMS resonant cantilevers for ultrasensitive biological detection, J. Sens. (2009).
[2] B. Arash, Q. Wang, Detection of gas atoms with carbon nanotubes, Sci. Rep. 3 (2013) 1782.
[3] J. Chaste, A. Eichler, J. Moser, G. Ceballos, R. Rurali, A. Bachtold, A nanomechanical mass sensor with yoctogram resolution, Nat. Nanotechnol. 7 (5) (2012) 301.
[4] N.V. Lavrik, P.G. Datskos, Femtogram mass detection using photothermally actuated nanomechanical resonators, Appl. Phys. Lett. 82 (16) (2003) 2697–2699.
[5] G. Rius, F. Pérez-Múrano, Nanocantilever Beams: Modeling, Fabrication, and Applications, CRC Press, 2015, Ch. Nanocantilever beam fabrication for CMOS technology integration.
[6] A. Morassi, M. Dilena, On point mass identification in rods and beams from minimal frequency measurements, Inverse Prob. Eng. 10 (2002) 183–201.
[7] L. Rubio, J. Fernández-Sáez, A. Morassi, Point mass identification in rectangular plates from minimal natural frequency data, Mech. Syst. Signal Process. 80 (2016) 245–261.
[8] L. Rubio, J. Fernández-Sáez, A. Morassi, Crack identification in non-uniform rods by two frequency data, Int. J. Solids Struct. 75–76 (2015) 61–80.
[9] J. Fernández-Sáez, A. Morassi, M. Pressacco, L. Rubio, Unique determination of a single crack in a uniform simply supported beam in bending vibration, J. Sound Vib. 371 (2016) 94–109.
[10] A. Bouchaala, A.H. Nayfeh, N. Jaber, M.I. Younis, Mass and position determination in MEMS mass sensors: a theoretical and an experimental investigation, J. Micromech. Microeng. 26 (10) (2016) 105009.
[11] S. Cuenot, S. Demoustier-Champagne, B. Nysten, Elastic modulus of polypyrrole nanotubes, Phys. Rev. Lett. 85 (8) (2000) 1690.
[12] D.C.C. Lam, F. Yang, A.C.M. Chong, J. Wang, P. Tong, Experiments and theory in strain gradient elasticity, J. Mech. Phys. Solids 51 (2003) 1477–1508.
[13] S. Cuenot, C. Frétigny, S. Demoustier-Champagne, B. Nysten, Surface tension effect on the mechanical properties of nanomaterials measured by atomic force microscopy, Phys. Rev. B 69 (16) (2004) 165410.
[14] C. Chen, Y. Shi, Y.S. Zhang, J. Zhu, Y. Yan, Size dependence of Young's modulus in ZnO nanowires, Phys. Rev. Lett. 96 (7) (2006) 075505.
[15] R.A. Toupin, Elastic materials with couple-stresses, Arch. Ration. Mech. Anal. 11 (5) (1962) 385–414.
[16] R.D. Mindlin, Micro-structure in linear elasticity, Arch. Ration. Mech. Anal. 16 (1964) 51–78.
[17] R.D. Mindlin, Second gradient of strain and surface-tension in linear elasticity, Int. J. Solids Struct. 1 (1965) 417–438.
[18] F. Yang, A. Chong, D. Lam, P. Tong, Couple stress based strain gradient theory for elasticity, Int. J. Solids Struct. 39 (2002) 2731–2743.
[19] N.A. Fleck, J.W. Hutchinson, Strain gradient plasticity, Adv. Appl. Mech. 33 (1997) 295–361.
[20] H.T. Thai, T.P. Vo, T.K. Nguyen, S.E. Kim, A review of continuum mechanics models for size-dependent analysis of beams and plates, Compos. Struct. 177 (2017) 196–219.
[21] A. Morassi, J. Fernández-Sáez, R. Zaera, J.A. Loya, Resonator-based detection in nanorods, Mech. Syst. Signal Process. 93 (2017) 645–660.
[22] M. Dilena, M. Fedele Dell'Oste, J. Fernández-Sáez, A. Morassi, R. Zaera, Mass detection in nanobeams from bending resonant frequency shifts, Mech. Syst. Signal Process. 116 (2019) 261–276.
[23] J. Fernández-Sáez, A. Morassi, L. Rubio, R. Zaera, Transverse free vibration of resonant nanoplate mass sensors: identification of an attached point mass, Int. J. Mech. Sci. 150 (2019) 217–225.
[24] M.S. Hanay, S.I. Kelber, C.D. O'Connell, P. Mulvaney, J.E. Sader, M.L. Roukes, Inertial imaging with nanomechanical systems, Nat. Nanotechnol. 10 (4) (2015) 339.
[25] A.M. Bouchaala, Size effect of a uniformly distributed added mass on a nanoelectromechanical resonator, Microsyst. Technol. 24 (6) (2018) 2765–2774.
[26] H. Hochstadt, B. Lieberman, An inverse Sturm-Liouville problem with mixed given data, SIAM J. Appl. Math. 34 (4) (1978) 676–680.
[27] H. Hochstadt, On inverse problems associated with Sturm-Liouville operators, J. Differ. Eqs. 17 (1975) 220–235.
[28] V. Barcilon, On the uniqueness of inverse eigenvalue problems, Geophys. J. R. Astronaut. Soc. 39 (1974) 287–298.
[29] G. Gladwell, Inverse Problems in Vibration, 2nd edn., Kluwer, Dordrecht, The Netherlands, 2004.
[30] A. Schueller, Uniqueness for near-constant data in fourth-order inverse eigenvalue problems, J. Math. Anal. Appl. 258 (2001) 658–670.
[31] L. Caudill, P. Perry, A. Schueller, Isospectral sets for fourth-order ordinary differential operators, SIAM J. Math. Anal. 29 (4) (1998) 935–966.
[32] O.H. Hald, The inverse Sturm-Liouville problem with symmetrical potentials, Acta Math 141 (1978) 263–291.
[33] D.C. Barnes, The inverse eigenvalue problem with finite data, SIAM J. Math. Anal. 22 (3) (1991) 732–753.
[34] A. Morassi, Damage detection and generalized Fourier coefficients, J. Sound Vib. 302 (1–2) (2007) 229–259.

[35] G. Borg, Eine Umkehrung der Sturm-Liouvilleschen Eigenwertaufgabe. Bestimmung der Differentialgleichung durch die Eigenwerte, Acta Math. 78 (1946) 1–96.
[36] O.H. Hald, The inverse Sturm-Liouville problem and the Rayleigh-Ritz method, Math. Comput. 32 (143) (1978) 687–705.
[37] R. Knobel, B. Lowe, An inverse Sturm-Liouville problem for an impedance, Z. Angew Math. Phys. 44 (1993) 433–450.
[38] B. Akgöz, Ö. Civalek, Longitudinal vibration analysis for microbars based on strain gradient elasticity theory, J. Vib. Control 20 (2014) 606–616.
[39] M. Kahrobaiyan, M. Asghari, M. Ahmadian, Longitudinal behavior of strain gradient bars, Int. J. Eng. Sci. 66 (2013) 44–59.
[40] H. Brezis, Analisi Funzionale, Liguore Editore, Napoli, Italia, 1986.
[41] R. Courant, D. Hilbert, Methods of Mathematical Physics, first English edition., Interscience Publishers Inc., New York, 1966.
[42] H. Weinberger, A First Course in Partial Differential Equations, Dover Publications Inc., New York, USA, 1965.
[43] S. Kong, S. Zhou, Z. Nie, K. Wang, Static and dynamic analysis of micro-beams based on strain gradient elasticity theory, Int. J. Eng. Sci. 47 (2009) 487–498.
[44] D. Calvetti, L. Reichel, D. Sorensen, An implicitly restarted Lanczos method for large symmetric eigenvalue problems, Electron. Trans. Numer. Anal. 2 (1994) 1–21.
[45] W. Rundell, P. Sacks, The reconstruction of Sturm-Liouville problems, Inverse Prob. 8 (3) (1992) 457–482.
[46] N. Rohrl, A least-squares functional for solving inverse Sturm-Liouville problems, Inverse Prob. 21 (2005) 2009–2017.
[47] A. Bilotta, A. Morassi, E. Turco, The use of quasi-isospectral operators for damage detection in rods, Meccanica 53 (2018) 319–345.